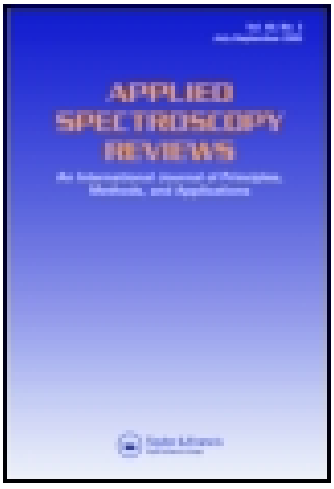

Applied Spectroscopy Reviews
Publication details, including instructions for authors and subscription information:
http://www.tandfonline.com/loi/laps20

Fourier Transform Infrared (FTIR) Spectroscopy of Biological Tissues

Zanyar Movasaghi [a], Shazza Rehman [b] & Dr. Ihtesham ur Rehman [a]
[a] Department of Materials, Interdisciplinary Research Centre in Biomedical Materials, School of Engineering and Material Sciences, Queen Mary University of London, London, UK
[b] Department of Medical Oncology, Guy's and St Thomas' Hospital NHS Foundation Trust, London, UK
Published online: 04 Feb 2008.

To cite this article: Zanyar Movasaghi, Shazza Rehman & Dr. Ihtesham ur Rehman (2008) Fourier Transform Infrared (FTIR) Spectroscopy of Biological Tissues, Applied Spectroscopy Reviews, 43:2, 134-179, DOI: 10.1080/05704920701829043

To link to this article: http://dx.doi.org/10.1080/05704920701829043

Applied Spectroscopy Reviews, 43: 134–179, 2008

ISSN 0570-4928 print/1520-569X online
DOI: 10.1080/05704920701829043

Fourier Transform Infrared (FTIR) Spectroscopy of Biological Tissues

Zanyar Movasaghi,[1] Shazza Rehman,[2] and Ihtesham ur Rehman[1]

[1]Department of Materials, Interdisciplinary Research Centre in Biomedical Materials, School of Engineering and Material Sciences, Queen Mary University of London, London, UK
[2]Department of Medical Oncology, Guy's and St Thomas' Hospital NHS Foundation Trust, London, UK

Abstract: This article reviews some of the recent advances on FTIR spectroscopy in areas related to natural tissues and cell biology. It is the second review publication resulting from a detailed study on the applications of spectroscopic methods in biological studies and summarizes some of the most widely used peak frequencies and their assignments. The aim of these studies is to prepare a database of molecular fingerprints, which will help researchers in defining the chemical structure of the biological tissues introducing most of the important peaks present in the natural tissues. In spite of applying different methods, there seems to be a considerable similarity in defining the peaks of identical areas of the FTIR spectra. As a result, it is believed that preparing a unique collection of the frequencies encountered in FTIR spectroscopic studies can lead to significant improvements both in the quantity and quality of research and their outcomes. This article is the first review of its kind that provides a precise database on the most important FTIR characteristic peak frequencies for researchers aiming to analyze natural tissues by FTIR spectroscopy and will be of considerable assistance to those who are focusing on the analysis of cancerous tissues by FTIR spectroscopy.

Keywords: FTIR spectroscopy, biological tissues, analysis of cancer tissues, characteristic peak assignments

Address correspondence to Dr. Ihtesham ur Rehman, Department of Materials, Interdisciplinary Research Centre in Biomedical Materials, School of Engineering and Material Sciences, Queen Mary University of London, Mile End Road, London E1 4NS, UK. E-mail: i.u.rehman@qmul.ac.uk

AIM OF THIS STUDY

The vibrational spectroscopic techniques, including FTIR spectroscopy, are potential tools for noninvasive optical tissue diagnosis. In recent years, applications of spectroscopic techniques in biological studies have increased a great deal, and particularly clinical investigations related to malignancy and cancer detection by spectroscopic means have attracted attention both by the clinical and non-clinical researchers.

Several papers have been published on the diagnostic importance of different spectroscopic and imaging techniques in the area of cancer detection (1–12). However, there is a gap, as it appears that the details of the characteristic peak frequencies and their definitions that can be attributed to specific functional groups present in the biological tissues have not been fully investigated. Furthermore, there is no paper to date that addresses the FTIR spectroscopic investigations of biological tissues, as researchers have to rely on a number of research papers and a majority of the time the interpretation of the spectral data differs significantly. In this article, a significant amount of spectroscopic investigation reported on biological tissues has been reviewed and reveals that there are striking similarities in defining different peak frequencies. As a result, creating a unique database, containing a detailed study on the works, different chemical bands, and their assignments of spectral bands could provide significant assistance to research groups focusing on spectroscopy. This, in turn, can lead to considerable improvements in the quality and quantity of the research done.

This article aims to present a wide and detailed collection of interpretation of FTIR spectral frequencies. It is envisaged that this article will be of significant assistance to research groups working on FTIR spectroscopy of biological tissues.

INTRODUCTION

Recently, spectroscopy has emerged as one of the major tools for biomedical applications and has made significant progress in the field of clinical evaluation. Research has been carried out on a number of natural tissues using spectroscopic techniques, including FTIR spectroscopy. These vibrational spectroscopic techniques are relatively simple, reproducible, nondestructive to the tissue, and only small amounts of material (micrograms to nanograms) with a minimum sample preparation are required. In addition, these techniques also provide molecular-level information allowing investigation of functional groups, bonding types, and molecular conformations. Spectral bands in vibrational spectra are molecule specific and provide direct information about the biochemical composition. These bands are relatively narrow, easy to resolve, and sensitive to molecular structure, conformation, and environment.

A considerably wide field of medical and biological studies has been covered by spectroscopic methods in recent years. It is strongly believed that in studies related to spectroscopic techniques, both the reliable experimental procedure and characterization of spectral peak positions and their assignment along with accurate peak detection and definition are of crucial importance. Although a number of scientists have used different techniques, it seems that there is a marked similarity in their spectral interpretation of comparable areas in their collected spectra.

These spectral interpretation investigations reported to date have been tabulated in Table 1, which provides a detailed account of spectral frequencies of the biological tissues.

FTIR SPECTROSCOPY

FTIR spectroscopy is a vibrational spectroscopic technique that can be used to optically probe the molecular changes associated with diseased tissues (13–15). The method is employed to find more conservative ways of analysis to measure characteristics within tumor tissue and cells that would allow accurate and precise assignment of the functional groups, bonding types, and molecular conformations. Spectral bands in vibrational spectra are molecule specific and provide direct information about the biochemical composition. FTIR peaks are relatively narrow and in many cases can be associated with the vibration of a particular chemical bond (or a single functional group) in the molecule (16, 17).

A detailed definition of Raman spectroscopy and its application in biological studies has been presented (18). Although Raman spectroscopy and FTIR are relevant techniques, with their respective spectra complementary to one another, there are some differences between these two techniques. Probably the most important difference is the type of samples that can be investigated by each of these methods. FTIR mainly deals with non-aqueous samples, while Raman is as effective with aqueous samples as it is with non-aqueous ones. This is because of the problem mostly taken place with FTIR spectroscopy; the problem is due to strong absorption bands of water (19–21). In Raman, however, fluorescence and the strong effect of glass (mostly as containers) are the most significant problems during analysis. Raman requires minimal sample preparation and can perform confocal imaging, whereas FTIR requires comparatively more sample preparation and does not have the ability of confocal imaging. Furthermore, the physical effect of infrared is created by absorption and mainly influences the dipole and ionic bands such as O-H, N-H, and C═O. Raman effect originates from scattering (emission of scattered light) and changing of the polarizability of covalent bands like C═C, C-S, S-S, and aromatics. In other words, FTIR spectroscopy is due to changes in dipole moment during molecular vibration, whereas Raman spectroscopy involves a change in polarizability

Table 1. The spectral interpretations

Peak	Assignment	Ref. no.
472/5 cm^{-1}	$C_\alpha = C_{\alpha'}$ torsion and C-OH_3 torsion of methoxy group (4)	(76)
521 cm^{-1}	$C_\alpha = C_{\alpha'}$ torsion and ring torsion of phenyl (1)	(76)
600–900 cm^{-1}	CH out-of-plane bending vibrations	(77)
606 cm^{-1}	Ring deformation of phenyl (1)	(76)
608 cm^{-1}	Ring deformation of phenyl (1)	(76)
635 cm^{-1}	OH out-of-plane bend (associated)	(78)
700–1000 cm^{-1}	Out-of-plane bending vibrations	(76)
793 cm^{-1}	Guanine in a *C_3'endo/syn* conformation in the *Z* conformation of DNA	(65)
802–5 cm^{-1}	Left-handed helix DNA (*Z* form)	(65)
805 cm^{-1}	*$C_{3'}$ endo/anti* (A-form helix) conformation	(65)
813 cm^{-1}	Ring CH deformation	(76)
829 cm^{-1}	C_2' endo conformation of sugar	(65)
831/3 cm^{-1}	C_2' endo conformation of sugar	(65)
835 cm^{-1}	*$C_{2'}$ endo/anti* (B-form helix) conformation	(65)
835–40 cm^{-1}	Left-handed helix DNA (*Z* form)	(65)
860 cm^{-1}	*$C_{3'}$ endo/anti* (A-form helix) conformation	(65)
868 cm^{-1}	Left-handed helix DNA (*Z* form)	(65)
878 cm^{-1}	*$C_{3'}$ endo/anti* (A-form helix) conformation	(65)
889 cm^{-1}	C-C, C-O deoxyribose	(79)
890 cm^{-1}	*$C_{3'}$ endo/anti* (A-form helix) conformation	(65)
	$C_{2'}$ endo/anti (B-form helix) conformation	(65)
892 cm^{-1}	C-C, C-O deoxyribose	(65)
	Fatty acid, saccharide (β)	
900–1300 cm^{-1}	Phosphodiester region	(26)
900–1350 cm^{-1}	Phosphodiester stretching bands region (for absorbances due to collagen and glycogen)	(53)
925–9 cm^{-1}	Left-handed helix DNA (*Z* form)	(65)
938 cm^{-1}	Unassigned	(26)
940 cm^{-1}	Carotenoid	(80)
960 cm^{-1}	Symmetric stretching vibration of $\nu_1 PO_4^{3-}$ (phosphate of HA)	(76)
961 cm^{-1}	C-O deoxyribose, C-C	(50)
963 cm^{-1}	δ(C═O) (polysaccharides, pectin)	(81)
963/4 cm^{-1}	C-C, C-O deoxyribose	(65)
964 cm^{-1}	C-C and C-O in deoxyribose of DNA of tumor cells	(65)
	C-O deoxyribose, C-C	(50)
965 cm^{-1}	C-O stretching of the phosphodiester and the ribose	(25)

(*continued*)

Table 1. Continued

Peak	Assignment	Ref. no.
966 cm^{-1}	C-O deoxyribose, C-C	(50)
	DNA	(31)
970 cm^{-1}	Symmetric stretching mode of dianionic phosphate monoesters of phosphorylated proteins or cellular nucleic acids	(82)
	DNA	(58)
971 cm^{-1}	$\nu PO_4 =$ of nucleic acids and proteins	(31)
	Symmetric stretching mode of dianionic phosphate monoester in phosphorylated proteins, such as phosvitin	(31, 82)
972 cm^{-1}	OCH_3 (polysaccharides, pectin)	(81)
985 cm^{-1}	OCH_3 (polysaccharides-cellulose)	(81)
994 cm^{-1}	C-O ribose, C-C	(50)
995 cm^{-1}	Ring breathing	(76)
996 cm^{-1}	C-O ribose, C-C	(50)
1000–50 cm^{-1}	Ring stretching vibrations mixed strongly with CH in-plane bending	(77)
1000–140 cm^{-1}	Protein amide I absorption	(56)
1000–150 cm^{-1}	A reasonably specific area for nucleic acids in the absence of glycogen	(25)
1000–200 cm^{-1}	C-OH bonds in oligosaccharides such as mannose & galactose	(51)
	Mainly from phosphate or oligosaccharide groups	(51)
	C-O stretching (carbohydrates)	(21)
1000–300 cm^{-1}	CH in-plane bending vibrations	(77)
	The aromatic CH bending and rocking vibrations	(76)
1000–350 cm^{-1}	Region of the phosphate vibration	(50)
	Carbohydrate residues attached to collagen and amide III vibration (in collagen)	(21)
1000–650 cm^{-1}	Porphyrin ring of heme proteins	(23)
1008 cm^{-1}	$CH_{\alpha,\alpha'}$ out-of-plane bending and $C_\alpha{=}C_{\alpha'}$ torsion	(76)
1009/10/1 cm^{-1}	Stretching C-O deoxyribose	(50)
1011 cm^{-1}	$CH_{\alpha,\alpha'}$ out-of-plane bending and $C_\alpha{=}C_{\alpha'}$ torsion	(76)
1018 cm^{-1}	ν(CO), ν(CC), δ(OCH), ring (polysaccharides, pectin)	(81)
1020 cm^{-1}	DNA	(53)
1020–50 cm^{-1}	Glycogen	(26)
1022 cm^{-1}	Glycogen	(26, 82)

(*continued*)

Table 1. Continued

Peak	Assignment	Ref. no.
1024 cm^{-1}	Glycogen (C-O stretch associated with glycogen)	(26, 82)
1025 cm^{-1}	Carbohydrates peak for solutions	(3)
	Vibrational frequency of -CH_2OH groups of carbohydrates (including glucose, fructose, glycogen, etc.)	(62)
	Glycogen	(3, 53)
	-CH_2OH groups and the C-O stretching vibration coupled with C-O bending of the C-OH groups of carbohydrates (including glucose, fructose, glycogen, etc.)	(54)
1028 cm^{-1}	Glycogen absorption due to C-O and C-C stretching and C-O-H deformation motions	(62)
1029/30 cm^{-1}	O-CH_3 stretching of methoxy groups	(76)
1030 cm^{-1}	Glycogen vibration	(33, 56)
	CH_2OH vibration	(33)
	ν_s C-O	(57)
	Collagen & phosphodiester groups of nucleic acids	(54)
1030 cm^{-1}	Stretching C-O ribose	(50)
1030 cm^{-1}	Collagen	(45)
1031 cm^{-1}	ν(CC) skeletal *cis* conformation, $\nu(CH_2OH)$, ν(CO) stretching coupled with C-O bending	(45, 61)
	Collagen	(31, 53)
	One of the triad peaks of nucleic acids (along with 1060 and 1081)	(25)
1032 cm^{-1}	O-CH_3 stretching of methoxy groups	(76)
1033 cm^{-1}	ν(CC) skeletal *cis* conformation, $\nu(CH_2OH)$, ν(CO) stretching coupled with C-O bending	(42, 45)
1034 cm^{-1}	Collagen	(21)
1035 cm^{-1}	Skeletal *trans* conformation (CC) of DNA	(62)
	ν(CC) skeletal *cis* conformation, $\nu(CH_2OH)$, ν(CO) stretching coupled with C-O bending	(45)
	Glycogen	(82)
	ν(CO), ν(CC), ν(CCO), (polysaccharides-cellulose)	(81)
1037 cm^{-1}	ν(CC) skeletal *cis* conformation, $\nu(CH_2OH)$, ν(CO) stretching coupled with C-O bending	(45)

(*continued*)

Table 1. Continued

Peak	Assignment	Ref. no.
1039/40 cm^{-1}	Stretching C-O ribose	(50)
1040–100 cm^{-1}	Symmetric PO_2^- stretching in RNA and DNA	(21)
1045 cm^{-1}	Glycogen band (due to OH stretching coupled with bending)	(34, 47)
	C-O stretching frequencies coupled with C-O bending frequencies of the C-OH groups of carbohydrates (including glucose, fructose, glycogen, etc.)	(62)
	-CH_2OH groups and the C-O stretching vibration coupled with C-O bending of the C-OH groups of carbohydrates (including glucose, fructose, glycogen, etc.)	(54)
1045/545 cm^{-1}	Gives an estimate carbohydrate concentrations (lower in malignant cells)	(54, 62)
1050 cm^{-1}	ν_s CO-O-C	(57)
	C-O stretching coupled with C-O bending of the C-OH of carbohydrates	(33)
	Glycogen	(26)
1050–70 cm^{-1}	C-O-C stretching (nucleic acids and phospholipids)	(21)
1050–80 cm^{-1}	Indicates a degree of oxidative damage to DNA	(53)
1050–100 cm^{-1}	Phosphate & oligosaccharides	(51)
	PO_2^- stretching modes, P-O-C antisymmetric stretching mode of phosphate ester, and C-OH stretching of oligosaccharides	(51)
1051 cm^{-1}	C-O-C stretching of DNA and RNA	(21)
1052 cm^{-1}	Phosphate I band for two different C-O vibrations of deoxyribose in DNA in *A* and *B* forms of helix or ordering structure	(65)
1053 cm^{-1}	νC-O & δC-O of carbohydrates	(31)
	Shoulder of 1121 cm^{-1} band, due to DNA	(55)
1055 cm^{-1}	Oligosaccharide C-O bond in hydroxyl group that might interact with some other membrane components	(51)
	Mainly from phospholipid phosphate and partly from oligosaccharide C-OH bonds	(51)
	Phosphate ester	(51)
	PO_2^- stretching and C-OH stretching of oligosaccharides	(51)

(*continued*)

Table 1. Continued

Peak	Assignment	Ref. no.
	Phosphate residues	(51)
	Membrane-bound oligosaccharide C-OH bond (a part of it may originate from the hydroxyl group of the sugar residue)	(51)
	ν(CO), ν(CC), δ(OCH) (polysaccharides, pectin)	(81)
1056/7 cm^{-1}	Stretching C-O deoxyribose	(50)
1059 cm^{-1}	2-Methylmannoside	(51)
	Oligosaccharide C-OH stretching band	(51)
	Mannose & mannose-6-phosphate	(51)
1060 cm^{-1}	Stretching C-O deoxyribose	(50)
	One of the triad peaks of nucleic acids (along with 1031 and 1081 cm^{-1})	(35)
	ν(CO), ν(CC), δ(OCH) (polysaccharides-cellulose)	(81)
1064 cm^{-1}	Stretching C-O ribose	(50)
1065 cm^{-1}	C-O stretching of the phosphodiester and the ribose	(25)
	Nucleic acids, in the absence of glycogen	(25)
1068 cm^{-1}	Stretching C-O ribose	(50)
1070 cm^{-1}	Mannose & mannose-6-phosphate	(51)
1070–80 cm^{-1}	Nucleic acid band	(83)
1071 cm^{-1}	Phosphate I band for two different C-O vibrations of Deoxyribose in DNA in disordering structure	(65)
1075 cm^{-1}	Symmetric phosphate stretching modes or $\nu(PO_2^-)$ sym. (phosphate stretching modes originate from the phosphodiester groups in nucleic acids and suggest an increase in the nucleic acids in the malignant tissues)	(45)
	$\nu(PO_2^-)$ symmetric stretching of phosphodiesters	(45)
1076 cm^{-1}	Skeletal *cis* conformation (CC) of DNA	(62)
1076 cm^{-1}	Symmetric phosphate [PO_2^- (sym)] stretching	(62)
1078 cm^{-1}	ν_s PO_2^-	(57)
	Phosphate I in RNA	(65)
	Symmetric phosphate	(26, 82)
	Glycogen absorption due to C-O and C-C stretching and C-O-H deformation motions	(25)

(*continued*)

Table 1. Continued

Peak	Assignment	Ref. no.
	DNA in healthy samples, in the absence of glycogen	(25)
	Indicating the role of phosphates during diseases	(58)
	C-OH stretching band of oligosaccharide residue	(51)
1079 cm^{-1}	ν_s PO_2^-	(26, 82)
1080 cm^{-1}	ν PO_2^-	(26, 35, 59)
	Phosphate vibration	(56)
	Symmetric phosphate [PO_2^- (sym)] stretching	(33)
	Collagen & phosphodiester groups of nucleic acids	(54)
1081 cm^{-1}	Symmetric phosphate stretching modes or $\nu(PO_2^-)$ sym. (phosphate stretching modes originate from the phosphodiester groups in nucleic acids and suggest an increase in the nucleic acids in the malignant tissues)	(45)
	$\nu(PO_2^-)$ symmetric stretching of phosphodiesters	(35)
	Phosphate I in RNA	(65)
	One of the triad peaks of nucleic acids (along with 1031 and 1060)	(25)
1082 cm^{-1}	PO_2^- symmetric	(52)
	Phosphate band	(60)
	Collagen	(53)
	Symmetric phosphate stretching band of the normal cells	(31)
1083 cm^{-1}	PO_2^- symmetric	(52)
1084 cm^{-1}	DNA (band due to PO_2^- vibrations)	(34)
	Symmetric phosphate [PO_2^- (sym)] stretching	(33, 53)
	PO_2^- symmetric	(52)
	Stretching PO_2^- symmetric	(65)
	Absorbance by the phosphodiester bonds of the phosphate/sugar backbone of nucleic acids	(53)
	Nucleic acid region	(53)
	Nucleic acid-phosphate band	(55)
1084–6 cm^{-1}	$\nu_s(PO_2^-)$ of nucleic acids	(31)
1085 cm^{-1}	PO_2^- symmetric (phosphate II)	(50)
	PO_2^- symmetric	(52)

(*continued*)

Table 1. Continued

Peak	Assignment	Ref. no.
	Mainly from absorption bands of the phosphodiester group of nucleic acids and membrane phospholipids, and partially protein (amide III). The band originating from sugar chains (C-OH band) overlaps.	(52)
	Mainly from phospholipid phosphate and partly from oligosaccharide C-OH bonds	(51)
	Phosphate ester	(51)
1086 cm^{-1}	Symmetric phosphate stretching modes or $\nu(PO_2^-)$ sym. (phosphate stretching modes originate from the phosphodiester groups in nucleic acids and suggest an increase in the nucleic acids in the malignant tissues)	(45)
	PO_2^- symmetric	(52)
	$\nu(PO_2^-)$ symmetric stretching of phosphodiesters	(35, 84)
1087 cm^{-1}	PO_2^- symmetric (phosphate II)	(50)
	Symmetric stretching of phosphate groups of phosphodiester linkages in DNA and RNA	(21)
	Symmetric PO_2^- stretching in RNA and DNA	(21)
	Symmetric stretching of phosphate groups in phospholipids	(21)
1088–90 cm^{-1}	Phosphate I (stretching PO_2^- symmetric vibration) in *B*-form DNA	(65)
1089 cm^{-1}	Stretching PO_2^- symmetric in RNA	(65)
1090 cm^{-1}	Mannose & mannose6-phosphate	(51)
	Phosphate ester (C-O-P) band	(51)
1090–100 cm^{-1}	Phosphate II (stretching PO_2^- asymmetric vibration) in *A*-form RNA	(65)
1094 cm^{-1}	Stretching PO_2^- symmetric (phosphate II)	(50)
	ν_{asym}(C-O-C) (polysaccharides-cellulose)	(81)
1095 cm^{-1}	Stretching PO_2^- symmetric	(25)
1099/100 cm^{-1}	Stretching PO_2^- symmetric (phosphate II)	(50)
1104 cm^{-1}	Symmetric stretching P-O-C	(50)
1105 cm^{-1}	Carbohydrates	(55)
1107 cm^{-1}	ν(CO), ν(CC), ring (polysaccharides, pectin)	(81)
1110 cm^{-1}	ν(CO), ν(CC) ring (polysaccharides, cellulose)	(81)
1113/5 cm^{-1}	Symmetric stretching P-O-C	(50)

(*continued*)

Table 1. Continued

Peak	Assignment	Ref. no.
1117 cm^{-1}	C-O stretching vibration of C-OH group of ribose (RNA)	(21)
1119 cm^{-1}	Symmetric stretching P-O-C	(50)
1119 cm^{-1}	C-O stretching mode	(82)
1120 cm^{-1}	Mannose-6-phosphate	(51)
	Phosphorylated saccharide residue	(51)
1121 cm^{-1}	Symmetric phosphodiester stretching band	(53)
	RNA	(53)
	Shoulder of 1121 cm^{-1} band, due to RNA	(55)
1122 cm^{-1}	νC-O of carbohydrates	(31)
1125 cm^{-1}	$CH_{2,6}$ in-plane bend and C_1-C_α-H_α bend	(75)
	ν(CO), ν(CC) ring (polysaccharides, cellulose)	(81)
1126 cm^{-1}	ν(C-O), disaccharides, sucrose	(81)
	ν(C-O)+ ν(C-C), disaccharides, sucrose	(81)
1137 cm^{-1}	Oligosaccharide C-OH stretching band	(51)
	2-Methylmannoside	(51)
1145 cm^{-1}	Phosphate & oligosaccharides	(51)
	Oligosaccharide C-O bond in hydroxyl group that might interact with some other membrane components	
	Membrane-bound oligosaccharide C-OH bond	
1150 cm^{-1}	C-O stretching vibration	(82)
	C-O stretching mode of the carbohydrates	(31)
	CH_8, CH_8'' deformations	(76)
	ν(C-O-C), ring (polysaccharides, pectin)	(81)
1150–200 cm^{-1}	Phosphodiester stretching bands (sym. and asym.)	(53)
1151 cm^{-1}	Glycogen absorption due to C-O and C-C stretching and C-O-H deformation motions	(25)
1152 cm^{-1}	CH_8, CH_8'' deformations	(76)
1153 cm^{-1}	Stretching vibrations of hydrogen-bonding C-OH groups	(33)
1155 cm^{-1}	C-O stretching vibration	(26)
	ν (C-C)-diagnostic for the presence of a carotenoid structure, most likely a cellular pigment	(64)
1159–74 cm^{-1}	νC-O of proteins and carbohydrates	(31)
1160 cm^{-1}	CO stretching	(33)
1161 cm^{-1}	Stretching vibrations of hydrogen-bonding C-OH groups	(33)

(*continued*)

Table 1. Continued

Peak	Assignment	Ref. no.
1161/2 cm^{-1}	Mainly from the C-O stretching mode of C-OH groups of serine, threosine, & tyrosine of proteins)	(45)
	ν(CC), δ(COH), ν(CO) stretching	(35, 41)
1162 cm^{-1}	Stretching modes of the C-OH groups of serine, threonine, and tyrosine residues of cellular proteins	(31)
	δ(C-O-C), ring (polysaccharides, cellulose)	(81)
1163 cm^{-1}	CH'_9, CH_7, CH'_7 deformations	(76)
1163/4 cm^{-1}	C-O stretching band of collagen (type I)	(52)
1164 cm^{-1}	Mainly from the C-O stretching mode of C-OH groups of serine, threosine, & tyrosine of proteins)	(35)
	ν(CC), δ(COH), ν(CO) stretching	(35, 42)
	C-O stretching (in normal tissue)	(60)
	Hydrogen-bonded stretching mode of C-OH groups	(31)
1170 cm^{-1}	ν_{as} CO-O-C	(57)
	C-O bands from glycomaterials and proteins	(52)
1172 cm^{-1}	Stretching vibrations of non-hydrogen-bonding C-OH groups	(33)
	CO stretching	(33)
	CO stretching of collagen (type I)	(52)
	Stretching modes of the C-OH groups of serine, threonine, and tyrosine residues of cellular proteins	(31)
1172/3 cm^{-1}	CO stretching of the C-OH groups of serine, threosine, & tyrosine in the cell proteins as well as carbohydrates	(33)
1173 cm^{-1}	C-O stretching (in malignant tissues)	(60)
1173 cm^{-1}	Non-hydrogen-bonded stretching mode of C-OH groups	(31)
1180–300 cm^{-1}	Amide III band region	(36)
1185/1/2 cm^{-1}	CH_2	(50)
1188 cm^{-1}	Deoxyribose	(50)
1200 cm^{-1}	Collagen	(45)
	Phosphate (P═O) band	(51)
1201 cm^{-1}	PO_2^- asymmetric (phosphate I)	(50)
1204 cm^{-1}	Vibrational modes of collagen proteins-amide III	(36)
	C-O-C, C-O dominated by the ring vibrations of polysaccharides C-O-P, P-O-P	(35, 43)

(*continued*)

Table 1. Continued

Peak	Assignment	Ref. no.
	Collagen	(28, 53)
1205 cm^{-1}	C-O-C, C-O dominated by the ring vibrations of polysaccharides C-O-P, P-O-P	(35, 45)
1206 cm^{-1}	Amide III	(25)
	Collagen	(31)
1207 cm^{-1}	PO_2^- asymmetric (phosphate I)	(25)
	Collagen	(21)
1209 cm^{-1}	PO_2^- asymmetric (phosphate I)	(50)
1212 cm^{-1}	PO_2^- asymmetric (phosphate I)	(50)
1217 cm^{-1}	PO_2^- asymmetric (phosphate I)	(50)
1220 cm^{-1}	PO_2^- asymmetric vibrations of nucleic acids when it is highly hydrogen-bonded	(33)
	Asymmetric hydrogen-bonded phosphate stretching mode	(31)
1220–4 cm^{-1}	Phosphate II (stretching PO_2^- asymmetric vibration) in *B*-form DNA	(65)
1220–40 cm^{-1}	Asymmetric PO_2^- stretching in RNA and DNA	(21)
1220–50 cm^{-1}	νPO_2^-	(59)
1220–350 cm^{-1}	Amide III (C-N stretching and N-H in plane bending, often with significant contributions from CH_2 wagging vibrations)	(21)
1222 cm^{-1}	Phosphate stretching bands from phosphodiester groups of cellular nucleic acids	(31)
	$CH_{6,2',\alpha,\alpha'}$ rock	(75)
1222/3 cm^{-1}	PO_2^- asymmetric (phosphate I)	(50, 85)
1224 cm^{-1}	Collagen	(21)
	Asymmetric stretching of phosphate groups of phosphodiester linkages in DNA and RNA	(21)
	Asymmetric PO_2^- stretching in RNA and DNA	(21)
	Symmetric stretching of phosphate groups in phospholipids	(21)
1226 cm^{-1}	PO_2^- asymmetric (phosphate I)	(50)
1230 cm^{-1}	Stretching PO_2^- asymmetric	(25, 65)
	Overlapping of the protein amide III and the nucleic acid phosphate vibration	(25)
1235 cm^{-1}	Composed of amide III as well as phosphate vibration of nucleic acids	(25)
	$CH_{6,2',\alpha,\alpha'}$ rock	(76)

(*continued*)

Table 1. Continued

Peak	Assignment	Ref. no.
1236 cm^{-1}	Amide III and asymmetric phosphodiester stretching mode ($\nu_{as}PO_2^-$), mainly from the nucleic acids	(36)
	$\nu_{as}PO_2^-$ of nucleic acids	(31)
1236–42 cm^{-1}	Relatively specific for collagen and nucleic acids	(53)
1236/7 cm^{-1}	Stretching PO_2^- asymmetric (phosphate I)	(50)
1237 cm^{-1}	PO_2^- asymmetric (phosphate I)	(50)
	PO_2^- asymmetric	(44)
1238 cm^{-1}	Stretching PO_2^- asymmetric (phosphate I)	(50)
	Asymmetric phosphate [PO_2^- (asym.)] stretching modes	(33)
	Stretching PO_2^- asymmetric	(65)
	Amide III	(25)
1238/9 cm^{-1}	Asymmetric PO_2^- stretching	(52)
1240 cm^{-1}	$\nu_{as}PO_2^-$	(26, 45)
	Collagen	(21, 31)
	Asymmetric non-hydrogen-bonded phosphate stretching mode (phosphate stretching modes originate from the phosphodiester groups of nucleic acids and suggest an increase in the nucleic acids in the malignant tissues)	(31)
	Mainly from absorption bands of the phosphodiester group of nucleic acids and membrane phospholipids, and partially protein (amide III)	(45)
	Amide III	(52)
	PO_2^- asymmetric vibrations of nucleic acids when it is non-hydrogen-bonded	(52)
	$\nu_{as}PO_2^-$	(33)
	Collagen	(57)
	Asymmetric phosphodiester stretching band	(53)
	Amide III	(53)
	PO_2^- ionized asymmetric stretching	(45)
	$\nu(PO_2^-)$ asymmetric stretching of phosphodiesters	(35, 62)
	Composed of amide III mode of collagen protein and the asymmetric stretching mode of the phosphodiester groups of nucleic acids	(26, 45, 47, 61)
	Asymmetric stretching mode of phosphodiester groups of nucleic acids	(31)

(*continued*)

Table 1. Continued

Peak	Assignment	Ref. no.
	Asymmetric PO_2^- stretching in RNA	(21, 31)
1240–45 cm^{-1}	Phosphate I (stretching PO_2^- symmetric vibration) in *A*-form RNA	(65)
1240–65 cm^{-1}	Amide III (C-N stretching mode of proteins, indicating mainly α-helix conformation)	(36, 86)
1240–310 cm^{-1}	νC-N, amide III	(59)
1241 cm^{-1}	PO_2^- asymmetric (phosphate I)	(50)
	Phosphate band (phosphate stretching modes originate from the phosphodiester groups of nucleic acids and suggest an increase in the nucleic acids in the malignant tissues; generally, the PO_2^- groups of phospholipids do not contribute to these bands)	(60)
	Phosphate stretching bands from phosphodiester groups of cellular nucleic acids	(33)
	ν_{as} Phosphate	(31), (35)
1242 cm^{-1}	PO_2^- asymmetric	(52)
	Collagen I & IV	(52)
	Amide III	(25, 53)
	Amide III collagen	31
1243 cm^{-1}	$\nu(PO_2^-)$ asymmetric stretching of phosphodiesters	(35, 84)
	Asymmetric phosphate [PO_2^- (asym.)] stretching modes (phosphate stretching modes originate from the phosphodiester groups of nucleic acids and suggest an increase the nucleic acids in the malignant tissues) (Generally, the PO_2^- groups of phospholipids do not contribute to these bands)	(33)
	Phosphate in RNA	(65)
1243/4 cm^{-1}	Collagen (type I)	(52)
1244 cm^{-1}	Collagen I & IV	(52)
	Asymmetric phosphate stretching ($\nu_{as}PO_2^-$)	(26, 65, 82)
1244/5 cm^{-1}	PO_2^- asymmetric (phosphate I)	(50)
1245 cm^{-1}	PO_2^- asymmetric	(52, 82)
1246 cm^{-1}	PO_2^- asymmetric	(26, 52)
1247 cm^{-1}	PO_2^- asymmetric (phosphate I)	(50)
1248 cm^{-1}	PO_2^- asymmetric	(52)
1250 cm^{-1}	Amide III	(64)
1250–400 cm^{-1}	CH_2 wagging vibration of the acyl chains (phospholipids)	(21)

(*continued*)

Table 1. Continued

Peak	Assignment	Ref. no.
1255 cm^{-1}	Amide III	(25)
1256 cm^{-1}	PO_2^- asymmetric (phosphate I	(50)
1262 cm^{-1}	PO_2^- asymmetric (phosphate I)	(50)
1265 cm^{-1}	PO_2^- asymmetric (phosphate I)	(50)
	$CH_{\alpha'}$ rocking	(76)
1272/3 cm^{-1}	$CH_{\alpha'}$ rocking	(76)
1276 cm^{-1}	N-H thymine	(50)
1278 cm^{-1}	Vibrational modes of collagen proteins-amide III	(36)
1278/9 cm^{-1}	Deformation N-H	(50)
1280 cm^{-1}	Collagen	(45)
	Amide III	(25)
1282 cm^{-1}	Amide III band components of proteins	(35, 45)
	Collagen	(21, 53)
1283 cm^{-1}	Collagen	(31)
1283–1339 cm^{-1}	Collagen	(31)
1284 cm^{-1}	Amide III band components of proteins	(41)
	Collagen	(21)
1287 cm^{-1}	Deformation N-H	(50)
1288 cm^{-1}	N-H thymine	(50)
1291/2 cm^{-1}	N-H thymine	(50)
1294/5/6 cm^{-1}	Deformation N-H cytosine	(50)
1306 cm^{-1}	Unassigned band	(82)
1307 cm^{-1}	Amide III	(25)
1310 cm^{-1}	Amide III	(59)
1312 cm^{-1}	Amide III band components of proteins	(35, 45)
1317 cm^{-1}	Amide III band components of proteins	(35, 45)
	Collagen	(31)
1327/8 cm^{-1}	Stretching C-N thymine, adenine	(50)
1328 cm^{-1}	Benzene ring mixed with the CH in-plane bending from the phenyl ring and the ethylene bridge	(76)
1330 cm^{-1}	CH_2 wagging	(35, 43)
1335 cm^{-1}	δ(CH), ring (polysaccharides, pectin)	(81)
1335 cm^{-1}	δ(CH), ring (polysaccharides, pectin)	(81)
1336 cm^{-1}	δ(CH), ring (polysaccharides, cellulose)	(81)
1337 cm^{-1}	Collagen	(53)
1337/8 cm^{-1}	CH_2 wagging	(35, 42, 47)
1339 cm^{-1}	Collagen	(31)
	In-plane C-O stretching vibration combined with the ring stretch of phenyl	76
1340 cm^{-1}	CH_2 wagging	(35, 45)
	Collagen	(21, 45)

(*continued*)

Table 1. Continued

Peak	Assignment	Ref. no.
1358 cm^{-1}	Stretching C-O, deformation C-H, deformation N-H	(50)
1367 cm^{-1}	Stretching C-O, deformation C-H, deformation N-H	(50)
1368 cm^{-1}	$\delta(CH_2)$, ν(CC) (polysaccharides, pectin)	(81)
1369/70 cm^{-1}	Stretching C-N cytosine, guanine	(50)
1370/1 cm^{-1}	Stretching C-O, deformation C-H, deformation N-H	(50)
1370/1/3 cm^{-1}	Deformation N-H, C-H	(65)
1373 cm^{-1}	Stretching C-N cytosine, guanine	(50)
1380 cm^{-1}	δCH_3	(57, 59)
	Stretching C-O, deformation C-H, deformation N-H	(50)
1390 cm^{-1}	Carbon particle	(25)
1395 cm^{-1}	Less characteristic, due to aliphatic side groups of the amino acid residues	(25)
1396 cm^{-1}	Symmetric CH_3 bending of the methyl groups of proteins	(33)
1398 cm^{-1}	CH_3 symmetric deformation	(87)
1399 cm^{-1}	Extremely weak peaks of DNA & RNA-arises mainly from the vibrational modes of methyl and methylene groups of proteins and lipids and amide groups	(33)
	Symmetric CH_3 bending modes of the methyl groups of proteins	(45)
	$\delta[(CH_3)]$ sym.	(44, 83)
	$\delta[C(CH_3)_2]$ symmetric	(35)
1400 cm^{-1}	Symmetric stretching vibration of COO^- group of fatty acids and amino acids	(82)
	$\delta_s CH_3$ of proteins	(31)
	Symmetric bending modes of methyl groups in skeletal proteins	(31)
	Specific absorption of proteins	(58)
	Symmetric stretch of methyl groups in proteins	(26)
1400–500 cm^{-1}	Ring stretching vibrations mixed strongly with CH in-plane bending	(76)
1400/1 cm^{-1}	COO^- symmetric stretching of acidic amino acids aspartate and glutamate	(21)
1400/1/2 cm^{-1}	CH_3 symmetric deformation	(87)
1401 cm^{-1}	Symmetric CH_3 bending modes of the methyl groups of proteins	(45)

(*continued*)

Table 1. Continued

Peak	Assignment	Ref. no.
	$\delta[(CH_3)]$ sym.	(44, 83)
	COO^- symmetric stretching of fatty acids	(21)
1401/2 cm^{-1}	Symmetric CH3 bending modes of the methyl groups of proteins	(45)
	$\delta[(CH_3)]$ sym.	(44, 45, 61)
	Stretching C-N, deformation N-H, deformation C-H	(50)
	$\delta[C(CH_3)_2]$ symmetric	(35)
1403 cm^{-1}	Symmetric CH_3 bending modes of the methyl groups of proteins	(45)
	$\delta[(CH3)]$ sym.	(42)
	$\delta_s CH_3$ of collagen	(31)
	$\delta[C(CH_3)_2]$ symmetric	(35)
1404/5 cm^{-1}	CH_3 asymmetric deformation	(87)
1412/4 cm^{-1}	Stretching C-N, deformation N-H, deformation C-H	(50)
1416 cm^{-1}	Deformation C-H, N-H, stretching C-N	(50)
1417 cm^{-1}	Stretching C-N, deformation N-H, deformation C-H	(50)
1418/9 cm^{-1}	Deformation C-H	(65)
1419 cm^{-1}	$\nu_s(COO^-)$ (polysaccharides, pectin)	(81)
1430 cm^{-1}	δ (CH_2) (polysaccharides, cellulose)	(81)
1444 cm^{-1}	$\delta(CH_2)$, lipids, fatty acids	(81)
	δ(CH) (polysaccharides, pectin)	(81)
1449 cm^{-1}	Asymmetric CH_3 bending of the methyl groups of proteins	(33)
1450 cm^{-1}	Methylene deformation in biomolecules	(82)
	Polyethylene methylene deformation modes	(25)
1451 cm^{-1}	Asymmetric CH_3 bending modes of the methyl groups of proteins	(45)
	$\delta[(CH_3)]$ asym.	(35, 44)
1454 cm^{-1}	Asymmetric methyl deformation	(26)
1455 cm^{-1}	C-O-H	(50)
	Less characteristic, due to aliphatic side groups of the amino acid residues	(25)
	$\delta_{as} CH_3$ of proteins	(31)
	Symmetric bending modes of methyl groups in skeletal proteins	(31)
1455/6 cm^{-1}	Asymmetric CH_3 bending modes of the methyl groups of proteins	(45)
	$\delta[(CH_3)]$ asym.	(35, 42, 45, 84)
1456 cm^{-1}	CH_3 bending vibration (lipids and proteins)	(21)

(*continued*)

Table 1. Continued

Peak	Assignment	Ref. no.
1457 cm^{-1}	Extremely weak peaks of DNA & RNA-arises mainly from the vibrational modes of methyl and methylene groups of proteins and lipids and amide groups	(33)
	Asymmetric CH_3 bending modes of the methyl groups of proteins	(45)
	$\delta[(CH_3)]$ asym.	(35, 42, 45, 84)
1458 cm^{-1}	$\delta_{as}CH_3$ of collagen	(31)
1462 cm^{-1}	Paraffin	(3)
1465 cm^{-1}	CH_2 scissoring mode of the acyl chain of lipid	(52)
1467 cm^{-1}	Cholesterol-methyl band	(34)
1468 cm^{-1}	δCH_2	(59)
	δCH_2 of lipids	(31)
	CH_2 bending vibration (lipids and proteins)	(21)
1469 cm^{-1}	CH_2 bending of the acyl chains of lipids	(33)
	CH_2 scissoring vibration of the acyl chains (phospholipids)	(21)
1470 cm^{-1}	CH_2 bending of the methylene chains in lipids	(88)
1480 cm^{-1}	Polyethylene methylene deformation modes	(25)
1480–543 cm^{-1}	Amide II	(81)
1480–600 cm^{-1}	The region of the amide II band in tissue proteins. Amide II mainly stems from the C-N stretching and C-N-H bending vibrations weakly coupled to the C=O stretching mode	(36)
1482 cm^{-1}	Benzene	(45)
1482/3/5 cm^{-1}	C_8-H coupled with a ring vibration of guanine	(50)
1486 cm^{-1}	Deformation C-H	(65)
1487/8 cm^{-1}	C=C, deformation C-H	(50)
1488/9 cm^{-1}	Deformation C-H	(65)
1489 cm^{-1}	In-plane CH bending vibration	(76)
1490 cm^{-1}	C=C, deformation C-H	(50)
	In-plane CH bending vibration	(76)
1494 cm^{-1}	In-plane CH bending vibration	(76)
1495/6 cm^{-1}	C=C, deformation C-H	(50)
1500 cm^{-1}	In-plane CH bending vibration from the phenyl rings	(76)
	CH in-plane bending	(76)
1500–60 cm^{-1}	Amide II (an N-H bending vibration coupled to C-N stretching	(21)

(*continued*)

Table 1. Continued

Peak	Assignment	Ref. no.
1504 cm^{-1}	In-plane CH bending vibration from the phenyl rings	(76)
1510 cm^{-1}	In-plane CH bending vibration from the phenyl rings	(76)
	CH in-plane bend	(76)
1514 cm^{-1}	ν(C═C)-diagnostic for the presence of a carotenoid structure, most likely a cellular pigment	(64)
1517 cm^{-1}	Amide II	(57)
1524 cm^{-1}	Stretching C═N, C═C	(50)
1526 cm^{-1}	C═N guanine	(50)
1527 cm^{-1}	Stretching C═N, C═C	(50)
1528 cm^{-1}	C═N guanine	(50)
152,829/30 cm^{-1}	C═N adenine, cytosine	(65)
1530 cm^{-1}	Stretching C═N, C═C	(50)
1531 cm^{-1}	Modified guanine?	(50)
1532 cm^{-1}	Stretching C═N, C═C	(50)
1534 cm^{-1}	Modified guanine	(50)
	Amide II	(35)
1535/7 cm^{-1}	Stretching C═N, C═C	(50)
1540 cm^{-1}	Protein amide II absorption- predominately β-sheet of amide II	(36)
	Amide II	(35)
1540–650 cm^{-1}	Amide II	(56)
1541 cm^{-1}	Amide II absorption (primarily an N-H bending coupled to a C-N stretching vibrational mode)	(26, 82)
	Amide II	(25)
1543 cm^{-1}	Amide II	(59)
1544 cm^{-1}	Amide II bands (arises from C-N stretching & CHN bending vibrations)	(62, 82)
1545 cm^{-1}	Protein band	(34)
	Amide II (δN-H, νC-N)	(57)
	Peptide amide II	(40, 58)
1549 cm^{-1}	Amide II	(35)
	Amide II of proteins	(31)
1550 cm^{-1}	Amide II	(83)
	Amide II of proteins	(52)
	N-H bending and C-N stretching	(48)
1550–650 cm^{-1}	Ring stretching vibrations with little interaction with CH in-plane bending	(77)
1550–800 cm^{-1}	Region of the base vibrations	(50)
1552 cm^{-1}	Ring base	(50)

(*continued*)

Table 1. Continued

Peak	Assignment	Ref. no.
1553 cm^{-1}	CO stretching	(33)
	Predominately α-sheet of amide II (Amide II band mainly stems from the C-N stretching and C-N-H bending vibrations weakly coupled to the C═O stretching mode)	(36)
1555 cm^{-1}	Ring base	(50)
1559 cm^{-1}	Ring base	(50)
1567 cm^{-1}	Ring base	(50)
1570 cm^{-1}	Amide II	(89)
1571/3 cm^{-1}	C═N adenine	(50)
1574/5 cm^{-1}	C═N adenine	(50)
1576 cm^{-1}	C═N adenine	(50)
1577 cm^{-1}	Ring C-C stretch of phenyl	(76)
1581 cm^{-1}	Ring C-C stretch of phenyl	(76)
1589 cm^{-1}	Ring C-C stretch of phenyl	(76)
1592 cm^{-1}	C═N, NH_2 adenine	(50)
1594 cm^{-1}	Ring C-C stretch of phenyl (2)	(50)
1596 cm^{-1}	Methylated nucleotides	(50)
1597 cm^{-1}	C═N, NH_2 adenine	(50)
1600–720 cm^{-1}	The region of the amide I band of tissue proteins (highly sensitive to the conformational changes in the secondary structure; amide I band is due to in-plane stretching of the C═O bond, weakly coupled to stretching of the C-N and in-plane bending of the N-H bond)	(36)
1600–800 cm^{-1}	C═O stretching (lipids)	(21)
1601/2 cm^{-1}	C═N cytosine, N-H adenine	(50)
1603/4 cm^{-1}	C═N, NH_2 adenine	(50)
1604 cm^{-1}	Adenine vibration in DNA	(65)
1605 cm^{-1}	ν_{as} (COO^-) (polysaccharides, pectin)	(81)
1606 cm^{-1}	Adenine vibration in DNA	(65)
1609 cm^{-1}	Adenine vibration in DNA	(65)
1618 cm^{-1}	Ring C-C stretch of phenyl	(76)
1620 cm^{-1}	Peak of nucleic acids due to the base carbonyl stretching and ring breathing mode	(25)
1630–700 cm^{-1}	Amide I region	(26)
1632 cm^{-1}	Ring C-C stretch of phenyl	(76)
1632/4 cm^{-1}	C═C uracyl, C═O	(50)
1635 cm^{-1}	β-sheet structure of amide I	(36)
	Proportion of β-sheet secondary structures (shoulder)	(21)

(*continued*)

Table 1. Continued

Peak	Assignment	Ref. no.
1637 cm^{-1}	C═C uracyl, C═O	(50)
1638/9 cm^{-1}	C═C thymine, adenine, N-H guanine	(50)
1639 cm^{-1}	Amide I	(35)
1640 cm^{-1}	Amide I band of protein and H-O-H deformation of water	(48)
1642 cm^{-1}	C_5 methylated cytosine	(50)
1643 cm^{-1}	Amide I band (arises from C═O stretching vibrations)	(62)
1644 cm^{-1}	Amide I	(35)
1646 cm^{-1}	Amide I	(83)
	C_5 methylated cytosine	(50)
	C═O, stretching C═C uracyl, NH_2 guanine	(50)
1647/8 cm^{-1}	Amide I in normal tissues-for cancer is in lower frequencies	(83)
1649 cm^{-1}	Unordered random coils and turns of amide I	(36)
	C═O, C═N, N-H of adenine, thymine, guanine, cytosine	(65)
	O-H bending (water)	(21)
1650 cm^{-1}	Amide I absorption (predominantly the C═O stretching vibration of the amide C═O)	(26, 82)
	Protein amide I absorption	50
	C═O, stretching C═C uracyl, NH_2 guanine	(40, 55)
	Peptide amide I	
1652 cm^{-1}	Amide I	(28)
1652/3 cm^{-1}	C_2═O cytosine	(50)
1653/4 cm^{-1}	C═O, C═N, N-H of adenine, thymine, guanine, cytosine	(65)
1655 cm^{-1}	Amide I (of proteins in α-helix conformation)	(51, 57)
	Amide I (ν C═O, δ C-N, δ N-H)	(50)
	C═O cytosine	(65)
	C═O, C═N, N-H of adenine, thymine, guanine, cytosine	(50)
	Peak of nucleic acids due to the base carbonyl stretching and ring breathing mode	(25)
	Amide I has some overlapping with the carbonyl stretching modes of nucleic acid	(31)
	Amide I (α-helix)	(81)
1656 cm^{-1}	Amide I	(59, 90)
	C_2═O cytosine	(50)
1657 cm^{-1}	α-helical structure of amide I	(36)

(*continued*)

Table 1. Continued

Peak	Assignment	Ref. no.
1658 cm^{-1}	C═O, stretching C═C uracyl, NH_2 guanine	(50)
	Amide I	(25)
1659 cm^{-1}	Amide I	(35)
1660 cm^{-1}	Amide I band	(64)
	ν(C═C) *cis*, lipids, fatty acids	(81)
1664/5 cm^{-1}	C═O Cytosine, uracyl	(50)
1665 cm^{-1}	Amide I (disordered structure-solvated)	(81)
1666 cm^{-1}	C═O stretching vibration of pyrimidine base	(21)
1670 cm^{-1}	Amide I (anti-parallel β-sheet)	(81)
	ν(C═C) *trans*, lipids, fatty acids	(81)
1679 cm^{-1}	Stretching C═O vibrations that are H-bonded (changes in the C═O stretching vibrations could be connected with destruction of old H-bonds and creation of the new ones)	(50)
	C═O guanine deformation N-H in plane	(50)
1680 cm^{-1}	Unordered random coils and turns of amide I	(36)
1681/4 cm^{-1}	C═O Guanine deformation N-H in plane	(50)
1684 cm^{-1}	C═O Guanine deformation N-H in plane	(50)
1685 cm^{-1}	Amide I (disordered structure-non-hydrogen bonded)	(81)
1690 cm^{-1}	Peak of nucleic acids due to the base carbonyl stretching and ring breathing mode	(25)
1694 cm^{-1}	A high frequency vibration of an antiparallel β-sheet of amide I (the amide I band is due to in-plane stretching of the C═O band weakly coupled to stretching of the C-N and in-plane bending of the N-H bond)	(36)
1698/9 cm^{-1}	C_2═O guanine	(50)
	N-H thymine	(50)
1700–15 cm^{-1}	The region of the bases	(65)
1700–800 cm^{-1}	Fatty acid esters	(51)
1700/2 cm^{-1}	C═O guanine	(50)
1702 cm^{-1}	C═O thymine	(50)
	Stretching C═O vibrations that are H-bonded (changes in the C═O stretching vaibrations could be connected with destruction of old H-bonds and creation of the new ones)	(50)
1706/7 cm^{-1}	C═O thymine	(50)

(*continued*)

Table 1. Continued

Peak	Assignment	Ref. no.
1707 cm^{-1}	C═O guanine	(50)
1708 cm^{-1}	C═O thymine	(50)
1712/9 cm^{-1}	C═O	(50)
1713/4/6 cm^{-1}	C═O thymine	(50)
1717 cm^{-1}	C═O thymine	(50)
	Amide I (arises from C═O stretching vibration)	(21)
	C═O stretching vibration of DNA and RNA	(21)
	C═O stretching vibration of purine base	(21)
1719 cm^{-1}	C═O	(50)
1725–45 cm^{-1}	C═O stretching band mode of the fatty acid ester	(51)
1728/9 cm^{-1}	C═O band	(51)
1730 cm^{-1}	Absorption band of fatty acid ester	(51)
	Fatty acid ester band	(51)
1736 cm^{-1}	C═O stretching (lipids)	(21)
1739 cm^{-1}	ν(C═O) (polysaccharides, hemicellulose)	(91)
1740 cm^{-1}	C═O	(53, 83)
	C═O stretching (lipids)	(21)
	Ester C═O stretching vibration (phospholipids)	(21)
1743 cm^{-1}	C═O stretching mode of lipids	(40)
1745 cm^{-1}	Ester group (C═O) vibration of triglycerides	(83)
	ν(C═O) (polysaccharides, pectin)	(81)
1750 cm^{-1}	ν(C═C) lipids, fatty acids	(81)
1997/2040/53/58 cm^{-1}	The band of second order	(50)
2100 cm^{-1}	A combination of hindered rotation and O-H bending (water)	(21)
2600 cm^{-1}	H-bonded NH vibration band	(65)
2633/678 cm^{-1}	Stretching N-H (NH_3^+)	(50)
2727/731 cm^{-1}	Stretching N-H (NH_3^+)	(50)
2761 cm^{-1}	CH_3 modes	(23)
2765/66/69/99 cm^{-1}	Stretching N-H (NH_3^+)	(50)
2800 cm^{-1}	Stretching N-H (NH_3^+)	(50)
2800–3000 cm^{-1}	C-H	(57)
	Lipid region	(21, 53)
	CH_3,CH_2-lipid and protein	(51)
2800–3100 cm^{-1}	C-H stretching vibrations of methyl (CH_3) & methylene (CH_2) groups & olefins	(83)

(*continued*)

Table 1. Continued

Peak	Assignment	Ref. no.
2800–3500 cm^{-1}	Cholesterol, phospholipids and creatine (higher in normal tissues)	(62)
	Stretching vibrations of CH_2 & CH_3 of phospholipids, cholesterol and creatine	(62)
2802/12/20/21/4/34 cm^{-1}	Stretching N-H (NH_3^+)	(50)
2834 cm^{-1}	Symmetric stretching of methoxy (1)	(76)
2836 cm^{-1}	Stretching N-H (NH_3^+)	(50)
2838 cm^{-1}	Stretching C-H	(50)
	Symmetric stretching of methoxy (3)	(76)
2846 cm^{-1}	Symmetric stretching of methoxy (4)	(76)
2848 cm^{-1}	Cholesterol, phospholipids, and creatine (higher in normal tissues)	(62)
	Stretching vibrations of CH_2 & CH_3 of phospholipids, cholesterol, and creatine	(62)
2849 cm^{-1}	Stretching C-H	(50)
2850 cm^{-1}	C-H stretching bands	(83)
	Stretching C-H	(50)
	ν_s CH_2, lipids, fatty acids	(81)
	CH_2 symmetric	
2851 cm^{-1}	Symmetric CH_2 stretch	(50)
2852 cm^{-1}	ν_s CH_2	(57)
	Symmetric stretching vibration of CH_2 of acyl chains (lipids)	(21)
2853 cm^{-1}	ν_s CH_2 of lipids	(31)
	Asymmetric CH_2 stretching mode of the methylene chains in membrane lipids	(31)
2860 cm^{-1}	Stretching C-H	(50)
2874 cm^{-1}	ν_s CH_3	(57)
	Stretching C-H, N-H	(76)
	Symmetric stretching vibration of CH_3 of acyl chains (lipids)	(21)
2884/85 cm^{-1}	Stretching C-H	(76)
2886/7/8/9/90 cm^{-1}	Stretching C-H	(76)
2893/4/6 cm^{-1}	CH_3 symmetric stretch	(87)
2916 cm^{-1}	Cholesterol, phospholipids and creatine (higher in normal tissues)	(62)
	Stretching vibrations of CH_2 & CH_3 of phospholipids, cholesterol and creatine	(62)
2917/8/9 cm^{-1}	Stretching C-H	(50)
2922 cm^{-1}	Asymmetric stretching vibration of CH_2 of acyl chains (lipids)	(21)

(*continued*)

Table 1. Continued

Peak	Assignment	Ref. no.
2923–33 cm^{-1}	C-H stretching bands in malignant tissues	(83)
2923/5 cm^{-1}	Stretching C-H	(50)
2925 cm^{-1}	C-H stretching bands in normal tissues	(83)
	ν_{as} CH_2 lipids	(31)
2928 cm^{-1}	Stretching C-H	(50)
2930 cm^{-1}	C-H stretching bands	(83)
	ν_{as} CH_2	(35)
2947/8 cm^{-1}	Stretching C-H	(50)
2951 cm^{-1}	Stretching C-H	(50)
2952 cm^{-1}	CH_3 asymmetric stretch	(87)
2951/3/5/6 cm^{-1}	Stretching C-H	(50)
2956 cm^{-1}	Asymmetric stretching vibration of CH_3 of acyl chains (lipids)	(21)
2959 cm^{-1}	C-H stretching	(83)
	ν_{as} CH_3 of lipids, DNA, and proteins	(31)
	Asymmetric stretching mode of the methyl groups from cellular proteins, nucleic acids and lipids	(31)
2960 cm^{-1}	ν_{as} CH_3	(57)
2963 cm^{-1}	CH_3 modes	(23)
2965 cm^{-1}	Stretching C-H	(50)
2970 cm^{-1}	ν_{as} CH_3, lipids, fatty acids	(81)
2975 cm^{-1}	Stretching N-H, stretching C-H	(50)
2984 cm^{-1}	$CH_{\alpha,\alpha'}$ stretch	(76)
2993/4 cm^{-1}	C-H ring	(50)
2994 cm^{-1}	$CH_{\alpha,\alpha'}$ stretch	(76)
2998/9 cm^{-1}	C-H ring	(50)
3000 cm^{-1}	C-H ring	(50)
	CH stretching vibrations (remain unaltered by the methoxy and hydroxyl substitution)	(76)
3000–600 cm^{-1}	N-H stretching	(36)
3000–700 cm^{-1}	O-H stretching (water)	(21)
3007 cm^{-1}	C-H	(83)
3007–10 cm^{-1}	=C-H groups that are related to olefins bands or unsaturated fatty acids (absent in cancer samples)	(83)
3008 cm^{-1}	C-H ring	(50)
	ν_{as} (=C-H), lipids, fatty acids	(81)
3015 cm^{-1}	ν=CH of lipids	(31)
3015/17/20 cm^{-1}	$CH_{2'}$ aromatic stretch	(76)
3021/2 cm^{-1}	C-H ring	(50)
3050 cm^{-1}	Amid B (N-H stretching)	(57)

(*continued*)

Table 1. Continued

Peak	Assignment	Ref. no.
3064 cm^{-1}	C_2 aromatic stretching	(76)
3070 cm^{-1}	Fermi-enhanced overtone of the amide II band (at 1550 cm^{-1})	(36)
3072/4 cm^{-1}	C-H ring	(50)
3074 cm^{-1}	CH stretching band of the phenyl rings	(76)
	C_2-CH_2 aromatic stretching	(76)
3075 cm^{-1}	Amide B bands steming from N-H stretching modes in proteins and nucleic acids	(50)
3078 cm^{-1}	C-H ring	(50)
3111/4/6 cm^{-1}	C-H ring	(50)
3163/82 cm^{-1}	Stretching N-H symmetric	(50)
3190 cm^{-1}	N-H stretching bands of mainly *cis*-ordered substructures	(36)
3194/5/7/9/ 200 cm^{-1}	Stretching N-H symmetric	(50)
3200–550 cm^{-1}	Symmetric and asymmetric vibrations attributed to water. So it would be better not to consider this region for detailed analysis	(62)
3201 cm^{-1}	Stretching N-H symmetric	(50)
3216/17/26 cm^{-1}	Stretching O-H symmetric	(50)
3273/87/89 cm^{-1}	Stretching O-H symmetric	(50)
3293 cm^{-1}	OH stretching (associated)	(76)
3295 cm^{-1}	Amid A (N-H stretching)	(57)
3300 cm^{-1}	Amide A bands steming from N-H stretching modes in proteins and nucleic acids	(36)
3301 cm^{-1}	Amide A band	(35)
3313 cm^{-1}	Amide A band	(35)
3320 cm^{-1}	NH band	(65)
3327 cm^{-1}	Stretching N-H asymmetric	(50)
3328 cm^{-1}	Amide A band	(35)
3330/5/7/9/ 43 cm^{-1}	Stretching N-H asymmetric	(50)
3350 cm^{-1}	O-H, N-H, C-H	(65)
3353 cm^{-1}	Stretching N-H asymmetric	(50)
3354 cm^{-1}	O-H, N-H, C-H	(65)
3359 cm^{-1}	Stretching N-H asymmetric	(50)
	O-H, N-H, C-H	(65)
3362 cm^{-1}	O-H, N-H, C-H	(65)
3396 cm^{-1}	Stretching O-H asymmetric	(50)
3401 cm^{-1}	O-H & N-H stretching vibrations (hydrogen bonding network may vary in the malignant tissues)	(83)

(*continued*)

Table 1. Continued

Peak	Assignment	Ref. no.
3410/16/20/ 22 cm^{-1}	Stretching O-H asymmetric	(50)
3430 cm^{-1}	N-H stretching bands of mainly *trans*-ordered substructures	(36)
3435/442 cm^{-1}	Stretching O-H asymmetric	(50)
3500–600 cm^{-1}	OH bonds	(65)
3506 cm^{-1}	OH stretching (free)	(75)
3524/28/42 cm^{-1}	Stretching O-H	(50)
3561 cm^{-1}	OH stretching (free)	(76)
3570/77/78/82/ 90/9 cm^{-1}	Stretching O-H	(50)
3611 cm^{-1}	O-H & N-H stretching vibrations (hydrogen bonding network may vary in the malignant tissues)	(83)

(22). Another difference existing between the techniques is their resolution. While Raman has lateral resolution of 1–2 μm and confocal resolution of 2.5 μm, FTIR does not provide the possibility of confocal resolution, and its lateral resolution is 10–20 μm (23).

FTIR SPECTROSCOPY BIOLOGICAL RESEARCH

A wide range of biological studies have been covered by FTIR analysis. These studies include cervix (24–32), lung (33–35), breast (21, 36–39), skin (40–44), gastrointestinal tissue (45–48), brain (49–51), oral tissue (52), lymphoid tissue (53), lymphocytes (childhood leukemia) (54), non-Hodgkin's lymphoma (55), prostate (56, 57), colon (58–61), fibroblasts (62), bacteria (63, 64), tumor cells (65), DNA (66), anti-cancer drug (67), tissue processing (68), cancer detection (69), tissue preservation (70) cytotoxicity and heating (71), plant tissue (72), gallstones (73), glucose measurement (74), and bone (75). This part of this article presents a brief summary of experimental procedure that has been applied by different research groups. It is believed that knowing what has been considered in Materials and Methods of different studies can lead to a better understanding of peak definitions obtained.

Wood et al. (24) reported on FTIR spectroscopy as a biodiagnostic tool for cervical cancer. The spectra of the normal epithelial cells illustrated intense glycogen bands at 1022 cm^{-1} and 1150 cm^{-1} and a pronounced symmetric phosphate stretch at 1078 cm^{-1}. The spectral features suggestive of dysplastic or malignant transformations were mainly pronounced

symmetric and asymmetric phosphate modes and a reduction in the glycogen band intensity. This study demonstrated the potential of the automated FTIR cervical screening technology in the clinical environment.

Chiriboga et al. (25) reported on differentiation and maturation of the epithelial cells in the human cervix using infrared spectroscopy. Different layers of human cervical squamous tissue, representing different cellular maturation stages, exhibited quite dissimilar spectral patterns. Thus, it was concluded that this technique presents a powerful tool to monitor cell maturation and differentiation. In addition, a proper interpretation of the state of health of cells exfoliated from such tissues would be obtained through a detailed understanding of the spectra of the individual layers.

Wood et al. (26) carried out an FTIR microspectroscopic investigation of cell types and potential confounding variables in screening for cervical malignancies. The aim of the study was to determine the effectiveness of infrared spectroscopy in the diagnosis of cervical cancer and dysplasia. It was found that leukocytes, and in particular lymphocytes, have spectral features in the phosphodiester region ($1300-900\,cm^{-1}$), suggestive of changes indicative of malignancy. The use of ethanol as a fixative and dehydrating agent resulted in retention of glycogen and thus minimized the spectral changes in the glycogen region due to sampling technique. Erythrocyte spectra exhibited a reduction in glycogen band intensity but could be discerned by a relatively low-intensity $\nu_s\ PO_2^-$ band. Endocervical mucin spectra exhibit a reduction glycogen band and a very pronounced $\nu_s\ PO_2^-$ band, which was similar in intensity to the corresponding band in HeLa $\nu_s\ PO_2^-$ cells.

Sindhuphak et al. (27) screened cervical cell samples of Thai women by using FTIR spectroscopy and compared the results to the histologic diagnosis. Two hundred seventy-five cervical cell specimens were received from patients undergoing hysterectomy. Histological examinations showed 108 abnormal cases and 167 abnormal cases. FTIR results versus histology showed sensitivity of 96.3% and specificity of 96.4%. False-negative and false-positive rates were 3.7 and 3.6%, respectively.

A study was conducted by Mordechai et al. (28) on formalin-fixed melanoma and cervical cancer by FTIR microspectroscopy (FTIR-MSP) to detect common biomarkers that occur in both types of cancer, distinguishing them from the respective non-malignant tissues. The spectra were analyzed for changes in levels of biomolecules such as RNA, DNA, phosphates, and carbohydrates. Whereas carbohydrate levels showed a good diagnostic potential for detection of cervical cancer, this was not the case for melanoma. However, variation of the RNA/DNA ratio as measured at $1121/1020\,cm^{-1}$ showed similar trends between non-malignant and malignant tissues in both types of cancer. The ratio was higher for malignant tissues in both types of cancer.

Chiriboga et al. (29) carried out a comparative study of spectra of biopsies of cervical squamous epithelium and of exfoliated cervical cells using infrared spectroscopy. A comparison of infrared absorption spectra obtained from the different layers of squamous epithelium from the human cervix and infrared

spectra obtained from exfoliated cervical cells was done. It was shown that the technique is a sensitive tool to monitor maturation and differentiation of human cervical cells. Therefore, it was concluded that this spectroscopic method provides new insights into the composition and state of health of exfoliated cells.

Wong et al. (30) carried out research on exfoliated cells and tissues from human endocervix and ectocervix by FTIR and ATR/FTIR spectroscopy. They measured the transmission infrared spectra of exfoliated endocervical mucin-producing columnar epithelial cells and the attenuated total reflectance (ATR) infrared spectra of the single-columnar cell layer on the endocervical tissues and compared with the corresponding infrared spectra of ectocervical squamous cells and squamous epithelium. The effects of the contaminated connective tissue on the infrared spectra of the endocervical columnar epithelial tissue demonstrated that ATR/FTIR is a more desirable method than the transmission method to obtain meaningful and good quality infrared spectra of tissue samples, particularly for samples consisting of thin layers of different types of tissues. Substantial differences in the infrared spectra between the columnar cells and squamous cells on the endocervical and ectocervical tissues, respectively, were evident. The strong glycogen bands in the infrared spectrum of the ectocervical squamous cells were absent in the spectrum of endocervical columnar cells. These spectral changes were similar to that observed in malignant squamous cells. Therefore, if the decrease in the intensity of the glycogen bands is used as the only criterion for the determination of the cellular abnormalities in the cervix, the presence of a large number of normal endocervical columnar cells in the cervical specimen would lead to a false result. Consequently, it was concluded that in addition to the glycogen bands, other features in the infrared spectra should be considered for evaluation of abnormalities in exfoliated cervical epithelial cells.

A pressure-tuning FTIR spectroscopic study of carcinogenesis in human endometrium was reported by Fung et al. (31). The spectra of normal tissues differed from those obtained for grade I and grade III adenocarcinoma. Changes in the spectra of malignant samples were observed in the symmetric and asymmetric stretching bands of the phosphodiester backbones of nucleic acids, the CH stretching region, the C-O stretching bands of the C-OH groups of carbohydrates and cellular protein residuals, and the pressure dependence of the CH_2 stretching mode. These spectral changes in the endometrium were reproducible. It was also found for the first time that the epithelium in the normal endometrium exhibits unique structural properties compared with the epithelium of other normal human tissues.

Wang et al. (33) focused on the microscopic FTIR studies of lung cancer cells in pleural fluid. The results demonstrate significant spectral differences between normal, lung cancer, and tuberculous cells. The most considerable differences were in the ratio of peak intensities of 1030 and 1080 cm^{-1} bonds (originated mainly in glycogen and phosphodiester groups of nucleic

acids). One of the important advantages of this method was the possibility of obtaining quick and reliable results.

The research of Yano et al. (34) was about direct measurement of human lung cancerous and non-cancerous tissues by FTIR microscopy, in order to answer the question of whether this technique can be used as a clinical tool or not. The corrected peak heights (H1045 and H1467) obtained from the bands at 1045 cm^{-1} and 1465 cm^{-1}, which are due to glycogen and cholesterol, were chosen for a quantitative evaluation of the malignancy. It was concluded that these peaks are an exceptionally useful factor for discrimination of the cancerous tissues from the non-cancerous ones. If the H1045/H1467 ratio from measured spectrum is larger than 1.4, it could be said with confidence that the tissue contains squamous cell carcinoma (SCC) or adenocarcinoma at least partially. Furthermore, they carried out the microscopic mapping of the tissues containing both cancerous and non-cancerous sections, demonstrating that the color map reflects small changes in the spatial distribution of cancer cells in the tissues.

Yang et al. (35) reported on tumor cell invasion by FTIR microspectroscopy. In this study, a three-dimensional artificial membrane using collagen type I, one of the main components of basal membranes of the lung tissue, was established in order to investigate tumor cell invasion of lung cancer. The mapping images obtained with FTIR microspectroscopy were validated with standard histological section analysis. The FTIR image produced using a single wave number at 1080 cm^{-1}, corresponding to PO_2^- groups in DNA from cells, correlated well with the histological section, which clearly revealed a cell layer and invading cells within the membrane. Furthermore, the peaks corresponding to amide A, I and II in the spectra of the invading cells shifted compared to the non-invading cells, which may relate to the changes in conformation and/or heterogeneity in the phenotype of the cells. The data presented in this study demonstrate that FTIR microspectroscopy can be a fast and reliable technique to assess tumor invasion in vitro.

Eckel et al. (36) analyzed the IR spectra of normal, hyperplasia, fibroadenoma, and carcinoma tissues of human breast. They worked on characteristic spectroscopic patterns in the proteins bands of the tissue. Some of the results of their experiments are as follows: (A) In carcinomatous tissues the bands in the region of 3000–3600 cm^{-1} shifted to lower frequencies. (B) The 3300 cm^{-1}/3075 cm^{-1} absorbance ratio was significantly higher for the fibroadenoma. (C) For the malignant tissues, the frequency of α-helix amide I band decreased, while the corresponding β-sheet amide I band frequency increased. (D) 1657 cm^{-1}/1635 cm^{-1} and 1553 cm^{-1}/1540 cm^{-1} absorbance ratios were the highest for fibroadenoma and carcinoma. (E) The 1680 cm^{-1}/1657 cm^{-1} absorbance ratio decreased significantly in the order of normal, hyperplasia, fibroadenoma, and carcinoma. (F) The 1651 cm^{-1}/1545 cm^{-1} absorbance ratio increased slightly for fibroadenoma and carcinoma. (G) The bands at 1204 cm^{-1} and 1278 cm^{-1}, assigned to the vibrational modes of the collagen, did not appear in the original spectra as

the resolved peaks and were distinctly stronger for the carcinoma tissues. (H) The 1657 cm^{-1}/1204 cm^{-1} and 1657 cm^{-1}/1278 cm^{-1} absorbance ratios, both yielding information on the relative content of collagen, increased in the order of normal, hyperplasia, carcinoma, and fibroadenoma.

The main focus area of the comparative infrared spectroscopic study of Fabian et al. (21) was on human breast tumors, human breast tumor cell lines, and xenografted human tumor cells. The results indicated that substantial differences exist on a macroscopic level between the tumors, tumor cell lines, and xenografted tumor cells, which are related to the presence of a significant connective tissue matrix in the tumors. On a macroscopic level, tumor cell xenografts appear, in spectroscopic terms, to be relatively homogenous with a relatively weak signature characteristic of connective tissue. Differences on a microscopic level between adjacent small (30 μm^2) areas of the same xenografted tumor could be detected, which were due to local variations in collagen content. In addition to variations in collagen content, variations in the deposition of microscopic fat droplets throughout both human and xenografted tumors could be detected. The results indicated the care with which infrared spectroscopic studies of tissues must be carried out to avoid incorrect interpretation of results due to an incomplete understanding of tissue pathology.

The study of Sukuta and Bruch (40) was on factor analysis of cancer FTIR evanescent wave fiberoptical (FTIR-FEW) spectra. The purpose of the research was to isolate pure biochemical compounds and spectra and to classify skin cancer tumors. Apart from fulfilling the primary goals, it was demonstrated that the combination of FTIR-FEW technique and chemical factor analysis has the potential of a clinical diagnostic tool.

Wong et al. (41) applied infrared spectroscopy combined with high pressure (pressure-tuning infrared spectroscopy) for studying the paired sections of basal cell carcinomas (BCC) and normal skin from 10 patients. In this study, atmospheric pressure IR spectra from BCC were dramatically different from those from the corresponding normal skin. Compared to their normal controls, BCCs displayed increased hydrogen bonding of the phosphodiester group of nucleic acids, decreased hydrogen bonding of the C-OH groups of proteins, increased intensity of the band at 972 cm^{-1}, a decreased intensity ratio between the CH_3 stretching and CH_2 stretching bands, and accumulation of unidentified carbohydrates.

Lucassen et al. (42) used attenuated total reflectance Fourier transform infrared (ATR-FTIR) spectroscopy to measure hydration of the stratum corneum. It was believed that the determination of the hydration state of the skin is necessary to obtain basic knowledge about the penetration and loss of water in the skin stratum corneum. In this study, direct band fitting of the water bending, combination, and OH stretch bands over the 4000–650 cm^{-1} wave number range were applied. Separate band fits of water, normal stratum corneum, and occluded hydrated stratum corneum spectra were obtained, yielding band parameters of the individual water contributions in the bending mode at 1640 cm^{-1}, the combination band at 2125 cm^{-1}, and

the OH stretches in the hydrated skin stratum corneum spectra. They concluded that band fit analysis of hydrated skin stratum corneum ATR-FTIR spectra offers the possibility for quantitative determination of individual water band parameters.

McIntosh et al. (43) used infrared spectroscopy to examine basal cell carcinoma to explore distinctive characteristics of basal cell carcinoma versus normal skin samples and other skin neoplasms. Spectra of epidermis, tumor, follicle sheath, and dermis were acquired from unstained frozen sections and analyzed qualitatively, by t-tests and by linear discriminant analyses. Dermal spectra were significantly different from the other skin components mainly due to absorptions from collagen in dermis. Spectra of normal epidermis and basal cell carcinoma were significantly different by virtue of subtle differences in protein structure and nucleic acid content. Linear discriminant analysis characterized spectra as arising from basal cell carcinoma, epidermis, or follicle sheath with 98.7% accuracy. Use of linear discriminant analysis accurately classified spectra as arising from epidermis overlying basal cell carcinoma versus epidermis overlying non-tumor–bearing skin in 98.0% of cases. Spectra of basal cell carcinoma, squamous cell carcinoma, nevi, and malignant melanoma were qualitatively similar. Distinction of basal cell carcinoma, squamous cell carcinoma, and melanocytic lesions by linear discriminant analyses, however, was 93.5% accurate. Therefore, spectral separation of abnormal versus normal tissue was achieved with high sensitivity and specificity (43).

Barry et al. (44) recorded Fourier transform (FT) Raman and infrared spectra of the outermost layer of human skin, the stratum corneum. Assignments consistent with the FT Raman vibrations were made for the first time and compared with assignments from the FTIR spectrum. The results demonstrated that FT Raman spectroscopy holds several advantages over FTIR in studies of human skin. The molecular and conformational nature of human skin, and modifications induced by drug or chemical treatments, may be assessed by FT Raman spectroscopy.

Fujioka et al. (45) reported on discrimination between normal and malignant human gastric tissues by FTIR spectroscopy. Their aim was to determine whether malignant and normal human gastric tissues can be distinguished by the technique. As a result, 22 out of 23 gastric tissue samples and 9 out of 12 gastric normal samples were correctly segregated, yielding 88.6% accuracy. Subsequently, they concluded that FTIR spectroscopy can be a useful tool for screening gastric cancer.

Weng et al. (46) studied tumors from stomach, small intestine, colon, rectum, liver, and other parts of the digestive system, with FTIR fiber optics and FT-Raman spectroscopic techniques. The spectra of samples were recorded on a Magna750 FTIR spectrometer with a mercury cadmium telluride detector (MCD) and mid-infrared optical fiber. The measurements were carried out by touching the sample with an attenuated total reflectance (ATR) probe. FT-Raman spectra of the samples were recorded on a 950

FT-Raman spectrometer. The results indicate that (i) the C═O stretching band of adipose can be observed in some normal tissues but is rarely found in malignant tissues, (ii) the relative intensities I_{1460}/I_{1400} are high for normal tissue but low for malignant tissue. For most normal tissues the intensities for the 1250 cm^{-1} band are stronger than for band around 1310 cm^{-1}, while the 1310 cm^{-1} band in malignant tissues is often stronger than the 1250 cm^{-1} bands.

In a study reported by Mordechai et al. (47), adenocarcinoma and normal colonic tissues were studied. FTIR microspectroscopy was employed to analyze thin tissue specimens and a direct comparison with normal histopathological analysis, which served as a gold reference. Several unique differences between normal and cancerous intestinal specimens were observed. The cancerous intestine showed weaker absorption strength over a wide region. In addition, IR absorption spectra from intestinal tissues (normal and cancerous) with other biological tissue samples were also effectively compared.

A diagnostic research was carried out by Li et al. (48), which aimed at classifying endoscopic gastric biopsies into healthy, gastritis, and malignancy through the use of FTIR spectroscopy. A total of 103 endoscopic samples, including 19 cases of cancer, 35 cases of chronic atrophic gastritis, 29 cases of chronic superficial gastritis, and 20 healthy samples, were investigated by ATR-FTIR. Significant differences were observed in FTIR spectra of these four types of gastric biopsies. It was demonstrated that the sensitivity of the method for healthy, superficial gastritis, atrophic gastritis, and gastric cancer was 90, 90, 66, and 74%, respectively. It was concluded that FTIR spectroscopy can be a useful technique for monitoring disease processes in gastric endoscopic biopsies (48).

Choo et al. (49) applied infrared spectra of human central nervous system tissue for diagnosis of Alzheimer's disease (AD). In addition, they presented a means of classifying the spectroscopic data non-subjectively using several multivariate methods. The results demonstrated that IR spectroscopy can potentially be used in the diagnosis of AD from autopsy tissue. It was shown that correct classification of white and grey matter from brains identified by standard pathological methods as heavily, moderately, and minimally involved can be achieved with success rates of greater than 90% using appropriate methods. Classification of tissue as either control or AD was achieved with a success rate of 100%.

FTIR spectra of RNA isolated from brain tumor (glioma) and DNA isolated from low-dose gamma-irradiated epididymis cells of rats from the Chernobyl accident zone were investigated by Dovbeshko et al. (50). The aim was to study nucleic acid damage and report on the existence of damage in the primary, secondary, and tertiary structure of nucleic acid, which seem to be connected with modification of bases and sugars, and redistribution of the H-bond network. It has also been reported that a great amount of statistical data and good mathematical approaches are needed for the use of these data as diagnostic criteria.

Yoshida et al. (51) measured the FTIR spectra of brain microsomal membranes prepared from rats fed under two dietary oil conditions with and without brightness-discrimination learning tasks: one group fed α-linolenate deficient oil (safflower oil) and the other group fed the sufficient oil (perilla oil) from mothers to offspring. The infrared spectra of microsomes under the two dietary conditions without the learning task showed no significant difference in the range $1000-3000\ cm^{-1}$. Only after the learning task were the infrared spectral differences noted between the microsomal membranes from both groups. Spectral differences were observed mainly in the absorption bands of fatty acid ester at around $1730\ cm^{-1}$ (sn-2 position), those of phosphate and oligosaccharides in the range of $1050-1100\ cm^{-1}$, and a band at around $1145\ cm^{-1}$. These results suggest changes in hydration of membrane surface and modification in oligosaccharide environment (removal or modification) of microsomes, which may be correlated in part with dietary oil–induced changes in learning performance.

Fukuyama et al. (52) used FTIR microscopy for studying the differences between oral squamous cell carcinoma and normal mucosa (normal gingival epithelium or normal subgingival tissue). The tissue spectra were compared with the purified human collagen and keratin. One half of every tissue specimen was measured with FTIR and the other half was investigated histologically. The obtained data suggested that this technique is applicable to clinical diagnostics.

Andrus and Strickland (53) used FTIR spectroscopy for cancer grading. Freeze-dried tissue samples from lymphoid tumors were studied. The absorbance ratio of $1121\ cm^{-1}/1020\ cm^{-1}$ increased, along with the emergence of an absorbance pulse at $1121\ cm^{-1}$, with increasing clinicopathological grade of malignant lymphoma. This study proposed the above ratio as an index of the cellular RNA/DNA ratio after subtraction of the overlapping absorbances, if present, due to collagen or glycogen. Absorbance attributable to collagen increased lymphoma grade and was greater in benign inflammatory tumors than in low-grade lymphomas. It was also suggested that the ratio trend may form the basis of a universal cancer grading parameter to assist with cancer treatment decisions and may also be useful in the analysis of cellular growth perturbation induced by drugs or other therapies.

Mordechai et al. (54) applied FTIR microscpectroscopy for the follow-up of childhood leukemia chemotherapy. A case study was presented where lymphocytes isolated from two children before and after the treatment were characterized using FTIR microspectroscopy. Significant changes in the spectral pattern in the $800-1800\ cm^{-1}$ region were found after the treatment. Preliminary analysis of the spectra revealed that the protein content decreased in the T-type acute lymphoblastic leukemia (ALL) patient before the treatment in comparison to the age-matched controls. It was shown that the chemotherapy treatment results in decreased nucleic acids, total carbohydrates, and cholesterol contents to a remarkable extent in both B and T-type ALL patients.

Andrus (55) collected the spectra of various grades of malignant non-Hodgkin's lymphoma. Structural changes to lipids and proteins in the wave number region of 2800–300 cm^{-1}, seen as increasing CH_3/CH_2 ratio and decreasing symmetric CH_2/asymmetric CH_2 ratio, were found to occur with increasing lymphoma grade. Rising ribose content (1121 cm^{-1}) was seen to correlate with rising 996/966 cm^{-1} ratio (an index of RNA/DNA) with increasing malignancy grade as well. It was concluded that this method can potentially be applied to clinical cancer grading or in vitro cancer treatment sensitivity testing.

In another study, Gazi et al. (56), applying FTIR microspectroscopy, could separate the paraffin-embedded tissues samples of benign and cancerous prostate. They could also separate the FTIR spectra of prostate cancer cell lines derived from different metastatic sites. It was found that the ratio of peak areas of 1030 and 1080 cm^{-1} (corresponding to glycogen and phosphate vibrations respectively) suggest a potential method for the differentiation of benign from malignant cells. It should be mentioned that the tissues were analyzed after mounting onto a BaF_2 plate and subsequent removal wax using Citroclear™ followed by acetone.

Paluszkiewicz (57) reported on human cancer prostate tissues using FTIR microspectroscopy and SRIXE techniques. The tissue samples were also analyzed by a histopathologist. In this research, differences between cancerous and non-cancerous parts of the analyzed tissues were observed for both methods.

Argov et al. (58) reported on FTIR microspectroscopic study of inflammatory bowel disease (IBD) as an intermediate stage between normal and cancer. In this work, FTIR microspectroscopy was used to evaluate IBD cases and to study the IR spectral characteristics with respect to cancer and normal tissues from formalin-fixed colonic biopsies from patients. IBD tissues could be segregated from cancer or normal ones using certain parameters such as phosphate content and RNA/DNA ratios. The results exhibited that FTIR microspectroscopy can detect biochemical changes in morphologically identical IBD and cancer tissues and suggest which cases of IBD may require further evaluation for carcinogenesis.

Richter et al. (59) used FTIR spectroscopy in combination with positron emission tomography to identify the tumor tissues. Thin tissue sections of human squamous carcinoma from hypopharynx and human colon adenocarcinoma grown in nude mice were investigated. Tumor tissues could successfully be identified by FTIR spectroscopy, while it was not possible to accomplish this with PET alone. On the other hand, PET permitted the noninvasive screening for suspicious tissues inside the body, which could not be achieved by FTIR.

Rigas et al. (60) applied FTIR spectroscopy to study the tissue sections of human colorectal cancer. Pairs of tissue samples from colorectal cancer and histologically normal mucosa 5–10 cm away from the tumor were obtained from 11 patients who underwent partial colectomy. All cancer specimens

displayed abnormal spectra compared with the corresponding normal tissues. These changes involved the phosphate and C-O stretching bands, the CH stretch region, and the pressure dependence of the CH_2 bending and C═O stretching modes. It was indicated that in colonic malignant tissue, there are changes in the degree of hydrogen-bonding of (i) oxygen atoms of the backbone of nucleic acids (increased); (ii) OH groups of serine, tyrosine, and threonine residues (any or all of them) of cell proteins (decreased); and (iii) the C═O groups of the acyl chains of membrane lipids (increased). In addition, it was shown that changes occurred in the structure of proteins and membrane lipids (as judged by the changes in their ratio of methyl to methylene groups) and in the packing and the conformational structure of the methylene chains of membrane lipids.

Rigas and Wong (61) studied seven human colon cell lines by infrared spectroscopy including study of several spectral parameters under high pressure (pressure tuning spectroscopy). The seven adenocarcinoma cell lines displayed almost all of the important spectroscopic features of colon cancer tissues: (a) increased hydrogen bonding of the phosphodiester groups of nucleic acids; (b) decreased hydrogen bonding of the C-OH groups of carbohydrates and proteins; (c) a prominent band at $972\,cm^{-1}$; and (d) a shift of the band normally appearing at $1082\,cm^{-1}$ to $1086\,cm^{-1}$. These cell lines differed spectroscopically from the colon cancer tissues in that: (a) they displayed a band at $991\,cm^{-1}$, which is weak in colon tissues; and (b) the packing and degree of disorder of membrane lipids were close to those observed in normal colonic tissues. They concluded that these findings (i) establish IR spectroscopy, used in combination with pressure tuning, as a useful method to address problems of tumor biology in cell culture systems; (ii) indicate that these cell lines offer a useful experimental model to explore the origin of the spectroscopic changes that we observed in colon cancer tissues; and (iii) support the idea that the malignant colonocyte is the likely source of all or most spectroscopic abnormalities of human colon cancer.

In vitro viral carcinogenesis was studied by Huleihel (62). In this study, FTIR microscopy was used to investigate spectral differences between normal and malignant fibroblasts transformed by retrovirus infection. Significant differences were observed between cancerous and normal cells. It was concluded that the contents of vital cellular metabolites were significantly lower in the transformed cells than in the normal cells. In addition, as an attempt to identify cellular components responsible for the spectral dissimilarities, they found considerable differences between DNA of normal and cancerous cells.

In a proof-of-concept study, Mossoba et al. (63) made an investigation on printing microarrays of bacteria for identification by infrared microscopy. They used the technique as a tool for rapid bacteria identification and could demonstrate its effectiveness.

According to a published paper by Naumann (64), FTIR and FT-NIR Raman spectra of intact microbial cells are highly specific, fingerprint-like

signatures that can be used to (i) discriminate between diverse microbial species and strains; (ii) detect in situ intracellular components or structures such as inclusion bodies, storage materials, or endospores; (iii) detect and quantify metabolically released CO_2 in response to various different substances; and (iv) characterize growth-dependent phenomena and cell drug interactions. Particularly interesting applications arise by means of a light microscope coupled to the spectrometer. FT-IR spectra of microcolonies containing less than 103 cells can be obtained from colony replica by a stamping technique that transfers microcolonies growing on culture plates to a special IR sample holder. FTIR and FT-NIR Raman spectroscopy can also be used in tandem to characterize medically important microorganisms.

Dovbeshko et al. (65) carried out an FTIR reflectance study on surface enhanced IR absorption of nucleic acids from tumor cells. The application of this method to nucleic acids isolated from tumor cells revealed some possible peculiarities of their structural organization, namely, the appearance of unusual sugar and base conformations, modification of the phosphate backbone, and redistribution of the H-bond net. The spectra of the RNA from the tumor cells showed more sensitivity to the grade of malignancy than the spectra of the DNA. After application of the anticancer drug doxorubicin to sensitive and resistant strains, the DNA isolated from these strains had different spectral features, especially in the region of the phosphate I and II bands.

Jalkanen et al. (66) used vibrational spectroscopy to study protein and DNA structure, hydration, and binding of biomolecules, as a combined theoretical and experimental approach. The systems studied systematically were the amino acids, peptides, and a variety of small molecules. The goal was to interpret the experimentally measured vibrational spectra for these molecules to the greatest extent possible and to understand the structure, function, and electronic properties of these molecules in their various environments. It was also believed that the application of different spectroscopic methods to biophysical and environmental assays is expanding, and therefore a true understanding of the phenomenon from a rigorous theoretical basis is required.

FTIR and NIR-FT Raman spectral features of the anti-cancer drug combretastatin-A4 were studied by Binoy et al. (67). The vibrational analysis showed that the molecule exhibits similar geometric behavior as *cis*-stilbene and has undergone steric repulsion resulting in phenyl ring twisting with respect to the ethylenic plane.

Faolin et al. (68) carried out a study examining the effects of tissue processing on human tissue sections using vibrational spectroscopy. This study investigated the effect of freezing, formalin fixation, wax embedding, and dewaxing. Spectra were recorded from tissue sections to examine biochemical changes before, during, and after processing with both Raman and FTIR spectroscopy. New peaks due to freezing and formalin fixation as well as shifts in the amide bands resulting from changes in protein conformation and possible cross-links were found. Residual wax peaks were observed clearly in the Raman spectra. In the FTIR spectra a single wax contribution was seen,

which may contaminate the characteristic CH_3 deformation band in biological tissue. This study confirmed that formalin-fixed paraffin processed (FFPP) sections have diagnostic potential.

Sahu and Mordechai (69) studied FTIR spectroscopy in cancer detection. The areas of focus were the distinction of premalignant and malignant cells and tissues from their normal state using specific parameters obtained from the spectra. It was concluded that while the method still requires pilot studies and designed clinical trials to ensure the applicability of such systems for cancer diagnosis, substantial progress has been made in incorporating advances in computational into the system to increase the sensitivity of the entire setup, making it an objective and sensitive technique suitable for automation to suit the demands of the medical community.

THE CHARACTERISTIC PEAK FREQUENCIES

It is believed that accurate peak definitions can have significant influence on reliability of the results provided through different spectroscopic techniques. Studies reported to date in the literature indicate that most of the scientists have mainly used the previously published articles in order to define the data acquired from the spectra collected. However, without having a reliable and detailed database that can cover most of the required peaks in the spectral range, it would be a time-consuming task to find the meanings of different unknown peak intensities. In biological studies, for instance, where a wide range of chemical bands and functional groups can be attributed to every single peak, finding appropriate meanings, which can demonstrate the clinical importance of the technique and achieved results, can be one of the most important steps in finalizing a spectroscopic research work. As a result, and with the aim of putting these shortages aside, a wide range of most frequently seen peaks in FTIR studies are presented in Table 1.

SUMMARY

FTIR spectroscopy has become a well-accepted and widely used method to characterize biological tissues. The technique of FTIR spectroscopy has become a technique of choice for scientists interested in finding the chemical structural properties of natural and synthetic tissues. Not surprisingly, an increasing number of research groups is showing interest in applying FTIR spectroscopy for different objectives and methodologies, and a considerable amount of time and financial resources are being allocated to this area. The information presented in this review can result in significant savings, particularly in terms of time that scientists, especially the non-spectroscopists, have to spend for defining spectral data. The literature compiled in this review will help in precise and speedy interpretation of the spectral data. The tabulated

part, which is the main and comprehensive part of this article, is presented in a way that will surely make it easy to follow for researchers and will help in understanding the important characteristic peaks that are present in FTIR spectra of biological tissues. It is envisaged that considering the type of samples being investigated and the chemical bands and functional groups that can possibly exist in the samples, the peak frequencies can be located in the table, and the appropriate interpretations could be made with confidence. Furthermore, having a detailed knowledge of the list of peaks that can be assigned to different biochemical compounds (such as lipids, proteins, or nucleic acids) would lead to a better correlation between the chemical structural and the medical aspects of spectroscopy. The lipid contents and the chemical structure of these compounds can be evaluated using peak frequencies at $2956\,cm^{-1}$ (asymmetric stretching vibration of CH_3 of acyl chains), $2922\,cm^{-1}$ (asymmetric stretching vibration of CH_2 of acyl chains), $2874\,cm^{-1}$ (symmetric stretching vibration of CH_3 of acyl chains), $2852\,cm^{-1}$ (symmetric stretching vibration of CH_2 of acyl chains), and $1600–1800\,cm^{-1}$ (C═O stretching). The specifications of protein contents of biological samples can also be understood from $1717\,cm^{-1}$ (amide I, arising from C═O stretching vibration), $1500–600\,cm^{-1}$ (amide II, N-H bending vibration coupled to C-N stretching), and $1220–1350\,cm^{-1}$ (amide III, C-N stretching and N-H in plane bending, often with significant contributions from CH_2 wagging vibrations). The peaks related to nucleic acids are as follows: $1717\,cm^{-1}$ (C═O stretching vibration of purine base), $1666\,cm^{-1}$ (C═O stretching vibration of pyrimidine base), $1220–1240\,cm^{-1}$ (asymmetric PO_2^- stretching), $1117\,cm^{-1}$ (C-O stretching vibration of C-OH group of ribose), $1040–100\,cm^{-1}$ (symmetric stretching of phosphate groups of phosphodiester linkages), and $1050–70\,cm^{-1}$ (C-O-C stretching) (21). However, it would be more useful to have further and continuous review of this field to improve this work on regular basis and to keep it updated to prepare a unique database that can be used for different methodologies. In addition to the different research topics being covered on a regular basis, this review may provide significant assistance not only to spectroscopists but also in areas related to biomaterials sciences, chemistry, and tissue engineering.

REFERENCES

1. Mahadevan-Jansen, A. and Richards-Kortum, R. (1997) Raman spectroscopy for cancer detection, 19th Int. Conf. IEEE EMBS, Chicago, Oct 30–Nov 2.
2. Hanlon, E.B., Manoharan, R., Koo, T.-W., Shafer, K.E., Motz, J.T., Fitzmaurice, M., Kramer, J.R., Itzkan, I., Dasari, R.R., and Feld, M.S. (2000) Prospects for in vivo Raman spectroscopy. *Physics in Medicine and Biology*, 45: 1–59.
3. Dukor, R.K. (2002) Vibrational spectroscopy in the detection of cancer. *Biomedical Applications*, 5: 3335–3359.

4. Choo-Smith, L.-P., Edwards, H.G.M., Endtz, H.P., Kros, J.M., Heule, F., Barr, H., Robinson, J.S., Jr., Bruining, H.A., and Pupells, G.J. (2002) Medical applications of Raman spectroscopy: from proof of principle to clinical implementation. *Biopolymers (Biospectroscopy)*, 67: 1–9.
5. Swinson, B., Jerjes, W., El-Maaytah, M., Norris, P., and Hopper, C. (2002) Optical techniques in diagnosis of head and neck malignancy. *Oral Oncology*, 42: 221–228.
6. Shaw, R.A. and Mantsch, H.H. (1999) Vibrational biospectroscopy: from plants to animals to humans. A historical perspective. *Journal of Molecular Structure*, 480–481: 1–13.
7. Petrich, W. (2001) Mid-infrared and Raman spectroscopy for medical diagnostics. *Applied Spectroscopy Reviews*, 36 (2&3): 181–237.
8. Zeng, H., McWilliams, A., and Lam, S. (2004) Optical spectroscopy and imaging for early lung cancer detection: a review. *Photodiagnosis and Photodinamic Therapy*, 1: 111–122.
9. Parker, M.F. (2005) Emerging technology in cervical cancer screening: spectroscopy. *Clinical Obstetrics and Gynecology*, 48 (1): 209–217.
10. Dekker, E. and Fockens, P. (2005) Advances in colonic imaging: new endoscopic imaging methods. *European Journal of Gasteroenterology and Hepatology*, 17 (8): 803–808.
11. Demos, S.G., Vogel, A.J., and Gandjbakhche, A.H. (2006) Advances in optical spectroscopy and imaging of breast lesions. *Journal of Mammary Gland Biology*, 11: 165–181.
12. Pitt, G.D., Batchelder, D.N., Bennett, R., Bormett, R.W., Hayward, I.P., Smith, B.J.E., Williams, K.P.J., Yang, Y.Y., Baldwin, K.J., and Webster, S. (2005) Engineering aspects and applications of the new Raman instrumentation. *IEE Proceedings-Science, Measurement and Technology*, 152 (6): 241–318.
13. Ellis, D.I. and Goodacre, R. (2006) Metabolic fingerprinting in disease diagnosis: biomedical applications of infrared and Raman spectroscopy. *Analyst*, 131: 875–885.
14. Choo-Smith, L.P., Maquelin, K., van Vreeswijk, T., Bruining, H.A., Puppels, G.J., Ngo Thi, N.A., Kirschner, C., Naumann, D., Ami, D., Villa, A.M., Orsini, F., Doglia, S.M., Lamfarraj, H., Sockalingum, G.D., Manfait, M., Allouch, P., and Endtz, H.P. (2001) Investigating microbial (micro)colony heterogeneity by vibrational spectroscopy. *Applied Environironmental Microbiology*, 67 (4): 1461–1469.
15. Kidder, L.H., Colarusso, P., Stewart, S.A., Levin, I.W., Appel, N.M., Lester, D.S., Pentchev, P.G., and Lewis, E.N. (1999) Infrared spectroscopic imaging of the biochemical modifications induced in the cerebellum of the Niemann–Pick type C mouse. *Journal of Biomedical Optics*, 4 (1): 7–13.
16. Kang, G.S., Ko, H.J., and Choi, C.K. (2003) Chemical bond structure of a-C:F films with a low dielectric constant deposited by using CH4/CF4 ICPCVD. *Journal of the Korean Physical Society*, 42 (5): 676–681.
17. Hofman, M., Pasieczna, S., Wachowski, L., and Ryczkowski, J. (2006) Speciation of functional groups formed on the surface of carbonaceous materials modified by NO. *Journal of Physics IV France*, 137: 287–290.
18. Movasaghi, Z., Rehman, S., and Rehman, I.U. (2007) Raman spectroscopy of biological tissues. *Applied Spectroscopy Reviews*, 42 (5): 493–541.
19. Mandeville, C.W., Webster, J.D., Rutherford, M.J., Taylor, B.E., Timbal, A., and Faure, K. (2002) Determination of molar absorptivities for infrared absorption bands of H_2O in andesitic glasses. *American Mineralogist*, 87: 813–821.

20. Seaman, S.J., Dyar, M.D., Marinkovic, N., and Dunbar, N.W. (2006) An FTIR study of hydrogen in anorthoclase and associated melt inclusions. *American Mineralogist*, 91: 12–20.
21. Fabian, H., Jackson, M., Murphy, L., Watson, P.H., Fichtner, I., and Mantsch, H.H. (1995) A comparative infrared spectroscopic study of human breast tumors and breast tumor cell xenografts. *Biospectroscopy*, 1 (1): 37–45.
22. Conroy, J., Ryder, A.G., Leger, M.N., Hennessey, K., and Madden, M.G. (2005) Qualitative and quantitative analysis of chlorinated solvents using Raman Spectroscopy and machine learning. *Proceedings of the International Society of Optical Engineers*, 5826: 131–142.
23. Alfano, R.R., Tang, G.C., Pradhan, A., Lam, W., Choy, D.S.J., and Opher, E. (1987) Optical spectroscopic diagnosis of cancer and normal breast tissues. *Journal of the Optical Society of America B*, 1987, 6 (5): 1015..
24. Wood, B.R., Quinn, M.A., Burden, F.R., and McNaughton, D. (1996) An investigation into FT-IR spectroscopy as a bio-diagnostic tool for cervical cancer. *Biospectroscopy*, 2: 143–153.
25. Chiriboga, L., Xie, P., Yee, H., Vigorita, V., Zarou, D., Zakim, D., and Diem, M. (1998) Infrared spectroscopy of human tissue. I. Differentiation and maturation of epithelial cells in the human cervix. *Biospectroscopy*, 4: 47–53.
26. Wood, B.R., Quinn, M.A., Tait, B., Ashdown, M., Hislop, T., Romeo, M., and McNaughton, D. (1998) FTIR microspectroscopic study of cell types and potential confounding variables in screening for cervical malignancies. *Biospectroscopy*, 4: 75–91.
27. Sindhuphak, R., Issaravanich, S., Udomprasertgul, V., Srisookho, P., Warakamin, S., Sindhuphak, S., Boonbundarlchai, R., and Dusitsin, N. (2003) A new approach for the detection of cervical cancer in Thai women. *Gynecologic Oncology*, 90: 10–14.
28. Mordechai, S., Sahu, R.K., Hammody, Z., Mark, S., Kantarovich, K., Guterman, H., Podshyvalov, J., Goldstein, J., and Argov, S. (2004) Possible common biomarkers from FTIR microspectroscopy of cervical cancer and melanoma. *Journal of Microscopy*, 215 (1): 86–91.
29. Chiriboga, L., Xie, P., Vigorita, V., Zarou, D., Zakin, D., and Diem, M. (1998) Infrared spectroscopy of human tissue. II. A comparative study of spectra of biopsies of cervical squamous epithelium and of exfoliated cervical cells. *Biospectroscopy*, 4: 55–59.
30. Wong, P.T.T., Lacelle, S., Fung, M.F.K., Senterman, M., and Mikhael, N.Z. (1995) Characterization of exfoliated cells and tissues from human endocervix and ectocervix by FTIR and ATR/FTIR spectroscopy. *Biospectroscopy*, 1 (5): 357–364.
31. Fung, M.F.K., Senterman, M.K., Mikhael, N.Z., Lacelle, S., and Wong, P.T.T. (1996) Pressure-tuning fourier transform infrared spectroscopic study of carcinogenesis in human endometrium. *Biospectroscopy*, 2: 155–165.
32. Utzinger, U.R.S., Heintzelman, D.L., Mahadevan-Jansen, A., Malpica, A., Follen, M., and Richards-Kortum, R. (2001) Near-infrared Raman spectroscopy for in vivo detection of cervical precancers. *Applied Spectroscopy*, 55 (8): 955–959.
33. Wang, H.P., Wang, H.-C., and Huang, Y.-J. (1997) Microscopic FTIR studies of lung cancer cells in pleural fluid. *Science of the Total Environment*, 204: 283–287.
34. Yano, K., Ohoshima, S., Grotou, Y., Kumaido, K., Moriguchi, T., and Katayama, H. (2000) Direct measurement of human lung cancerous and noncancerous tissues by fourier transform infrared microscopy: can an infrared microscope be used as a clinical tool? *Analytical Biochemistry*, 287: 218–225.

35. Yang, Y., Sule-Suso, J., Sockalingum, G.D., Kegelaer, G., Manfait, M., and El Haj, A.J. (2005) Study of tumor cell invasion by Fourier transform infrared microspectroscopy. *Biopolymers*, 78: 311–317.
36. Eckel, R., Huo, H., Guan, H.-W., Hu, X., Che, X., and Huang, W.-D. (2001) Characteristic infrared spectroscopic patterns in the protein bands of human breast cancer tissue. *Vibrational Spectroscopy*, 27: 165–173.
37. Kline, N.J. and Treado, P.J. (1997) Raman chemical imaging of breast tissue. *Journal of Raman Spectroscopy*, 28: 119–124.
38. Shafer-Peltier, K.E., Haka, A.S., Fitzmaurice, M., Crowe, J., Dasar, R.R., and Feld, M.S. (2002) Raman microspectroscopic model of human breast tissue: implications for breast cancer diagnosis in vivo. *Journal of Raman Spectroscopy*, 33: 552–563.
39. Frank, C.J., McCreecy, R.L., and Redd, D.C.B. (1995) Raman spectroscopy of normal and diseased human breast tissues. *Analytical Chemistry*, 67: 777–783.
40. Sukuta, S. and Bruch, R. (1999) Factor analysis of cancer Fourier transform infrared evanescent wave fiberoptical (FTIR-FEW) spectra. *Lasers in Surgery and Medicine*, 24: 382–388.
41. Wong, P.T.T., Goldstein, S.M., Grekin, R.C., Godwin, T.A., Pivik, C., and Rigas, B. Distinct infrared spectroscopic patterns of human basal cell carcinoma. *Cancer Research*, 53 (4): 762–765.
42. Lucassen, G.W., Van Veen, G.N., and Jansen, J.A. (1998) Band analysis of hydrated human skin stratum corneum attenuated total reflectance Fourier transform infrared spectra in vivo. *Journal of Biomedical Optics*, 3: 267–280.
43. McIntosh, L.M., Jackson, M., Mantsch, H.H., Stranc, M.F., Pilavdzic, D., and Crowson, A.N. (1999) Infrared spectra of basal cell carcinomas are distinct from non-tumor-bearing skin components. *Journal of Investigative Dermatology*, 112: 951–956.
44. Barry, B.W., Edwards, H.G.M., and Williams, A.C. (1992) Fourier transform Raman and infrared vibrational study of human skin: assignment of spectral bands. *Journal of Raman Spectroscopy*, 23: 641–645.
45. Fujioka, N., Morimoto, Y., Arai, T., and Kikuchi, M. (2004) Discrimination between normal and malignant human gastric tissues by Fourier transform infrared spectroscopy. *Cancer Detection & Prevention*, 28: 32–36.
46. Weng, S.F., Ling, X.F., Song, Y.Y., Xu, Y.Z., Li, W.H., Zhang, X., Yang, L., Sun, W., Zhou, X., and Wu, J. (2000) FT-IR fiber optics and FT-Raman spectroscopic studies for the diagnosis of cancer. *American Clinical Laboratory*, 19 (7): 20.
47. Mordechai, S., Salman, A.O., Argov, S., Cohen, B., Erukhimovitch, V., Goldstein, J., Chaims, O., and Hammody, Z. (2000) *Fourier-transform infrared* spectroscopy of human cancerous and normal intestine. *Proceedings of the SPIE*, 3918: 66–77.
48. Li, Q.B., Sun, X.J., Xu, Y.Z., Yang, L.M., Zhang, Y.F., Weng, S.F., Shi, J.S., and Wu, J.G. (2005) Diagnosis of gastric inflammation and malignancy in endoscopic biopsies based on Fourier transform infrared spectroscopy. *Clinical Chemistry*, 51 (2): 346–350.
49. Choo, L.-P., Mansfield, J.R., Pizzi, N., et al. (1995) Infrared spectra of human central nervous system tissue: Diagnosis of Alzheimer's disease by multivariate analyses. *Biospectroscopy*, 1 (2): 141–148.
50. Dovbeshko, G.I., Gridina, N.Y., Kruglova, E.B., and Pashchuk, O.P. (1997) FTIR spectroscopy studies of nucleic acid damage. *Talanta*, 53: 233–246.

51. Yoshida, S., Miyazaki, M., Sakai, K., Takeshita, M., Yuasa, S., Sato, A., Kobayashi, T., Watanabe, S., and Okuyama, H. (1997) Fourier transform infrared spectroscopic analysis of rat brain microsomal membranes modified by dietary fatty acids: possible correlation with altered learning behavior. *Biospectroscopy*, 3 (4): 281–290.
52. Fukuyama, Y., Yoshida, S., Yanagisawa, S., and Shimizu, M. (1999) A study on the differences between oral squamous cell carcinomas and normal oral mucosas measured by Fourier transform infrared spectroscopy. *Biospectroscopy*, 5: 117–126.
53. Andrus, P.G.L. and Strickland, R.D. (1998) Cancer grading by Fourier transform infrared spectroscopy. *Biospectroscopy*, 4: 37–46.
54. Mordechai, S., Mordechai, J., Ramesh, J., Levi, C., Huleihel, M., Erukhimovitch, V., Moser, A., and Kapelushnik, J. (2001) Application of FTIR microspectroscopy for the follow-up of childhood leukaemia chemotherapy, Proceedings of SPIE Subsurface and Surface Sensing Technologies and Applications III, 4491: 243–250.
55. Andrus, P.G. (2006) Cancer monitoring by FTIR spectroscopy. *Technology in Cancer Research and Treatment*, 5 (2): 157–167.
56. Gazi, E., Dwyer, J., Gardner, P., Ghanbari-Siakhani, A., Wde, A.P., Lockyer, N.P., Vickerman, J.C., Clarke, N.W., Shanks, J.H., Scott, L.J., Hart, C.A., and Brown, M. (2003) Applications of Fourier transform infrared microspectroscopy in studies of benign prostate and prostate cancer. A pilot study. *Journal of Pathology*, 201: 99–108.
57. Paluszkiewicz, C. and Kwiatek, W.M. (2001) Analysis of human cancer prostate tissues using FTIR microscopy and SXIXE techniques. *Journal of Molecular Structure*, : 565–566, 329–334.
58. Argov, S., Sahu, R.K., Bernshtain, E., Salam, A., Shohat, G., Zelig, U., and Mordechai, S. (2004) Inflammatory bowel diseases as an intermediate stage between normal and cancer: a FTIR-microspectroscopy approach. *Biopolymers*, 75: 384–392.
59. Richter, T., Steiner, G., Abu-Id, M.H., Salzer, R., Gergmann, R., Rodig, H., and Johannsen, B. (2002) Identification of tumor tissue by FTIR spectroscopy in combination with positron emission tomography. *Vibrational Spectroscopy*, 28: 103–110.
60. Rigas, B., Morgello, S., Goldman, I.S., and Wong, P.T.T. (1999) Human colorectal cancers display abnormal Fourier-transform infrared spectra, Proceedings of the National Academy of Sciences USA, 87: 8140–8144.
61. Rigas, B. and Wong, P.T.T. (1992) Human colon adenocarcinoma cell lines display infrared spectroscopic features of malignant colon tissues. *Cancer Research*, 52: 84–88.
62. Huleihel, M., Salman, A., Erukhimovich, V., Ramesh, J., Hammody, Z., and Mordechai, S. (2002) Novel optical method for study of viral carcinogenesis in vitro. *Journal of Biochemical and Biophysical Methods*, 50: 111–121.
63. Mossoba, M.M., Al-Khaldi, S.F., Kirkwood, J., Fry, F.S., Sedman, J., and Ismail, A.A. (2005) Printing microarrays of bacteria for identification by infrared microspectroscopy. *Vibrational Spectroscopy*, 38: 229–235.
64. Naumann, D. (1998) Infrared and NIR Raman spectroscopy in medical microbiology 3257: 245–257.
65. Dovbeshko, G.I., Chegel, V.I., Gridina, N.Y., Repnytska, O.P., Shirshov, Y.M., Tryndiak, V.P., Todor, I.M., and Solyanik, G.I. (2002) Surface enhanced IR

absorption of nucleic acids from tumor cells: FTIR reflectance study. *Biopolymer (Biospectroscopy)*, 67: 470–486.
66. Jalkanen, K.J., Würtz Jürgensen, V., Claussen, A., Rahim, A., Jensen, G.M., Wade, R.C., Nardi, F., Jung, C., Degtyarenko, I.M., Nieminen, R.M., Herrmann, F., Knapp-Mohammady, M., Niehaus, T.A., Frimand, K., and Suhai, S. (2006) Use of vibrational spectroscopy to study protein and DNA structure, hydration, and binding of biomolecules: A combined theoretical and experimental approach. *Journal of Quantum Chemistry*, 106: 1160–1198.
67. Binoy, J., Abraham, J.P., Joe, I.H., Jayakumar, V.S., Petit, G.R., and Nielsen, O.F. (2004) NIR-FT Raman and FT-IR spectral studies and ab initio calculations of the anti-cancer drug combretastatin-A4. *Journal of Raman Spectroscopy*, 35: 939–946.
68. Faolain, E.O., Hunter, M.B., Byrne, J.M., Kelehan, P., McNamer, M., Byrne, H.J., and Lyng, F.M. (2005) A study examining the effects of tissue processing on human tissue sections using vibrational spectroscopy. *Vibrational Spectroscopy*, 38: 121–127.
69. Sahu, P.K. and Mordechai, S. (2005) Fourier transform infrared spectroscopy in cancer detection. *Future Oncology*, 1: 635–647.
70. Pleshko, N.L., Boskey, A.L., and Mendelsohn, R. (1991) An FT-IR microscopic investigation of the effects of tissue preservation on bone. *Calcified Tissue International*, 51 (1): 72–77.
71. Holman, H.Y.N., Martin, M.C., and McKinney, W.R. (2003) Synchrotron-based FTIR spectromicroscopy: cytotoxicity and heating considerations. *Journal of Biological Physics*, 29 (2–3): 275–286.
72. Budevska, B.O., Sum, S.T., and Jones, T.J. (2003) Application of multivariate curve resolution for analysis of FT-IR microspectroscopic images of in situ plant tissue. *Applied Spectroscopy*, 57: 124–131.
73. Kleiner, O., Ramesh, J., Huleihel, M., Cohen, B., Kantarovich, K., Levi, C., Polyak, B., Marks, R.S., Mordehai, J., Cohen, Z., and Mordechai, S. (2002) A comparative study of gallstones from children and adults using FTIR spectroscopy and fluorescence microscopy. *BMC Gastroenterology*, 2: 3.
74. Tarumi, M., Shimada, M., Murakami, T., Tamura, M., Shimada, M., Arimoto, H., and Yamada, Y. (2003) Simulation study of in vitro glucose measurement by NIR spectroscopy and a method of error reduction. *Physics in Medicine and Biology*, 48: 2373–2390.
75. Smith, R. and Rehman, I.U. (1994) Fourier transform Raman spectroscopic studies of human bone. *Journal of Material Science; Materials in Medicine*, 5 (9&10): 775–778.
76. Schulz, H. and Baranska, M. (2007) Identification and qualification of valuable plant substances by IR and Raman spectroscopy. *Vibrational Spectroscopy*, 43: 13–25.
77. Chiang, H.-P., Song, R., Mou, B., Li, K.P., Chiang, P., Wang, D., Tse, W.S., and Ho, L.T. (1999) Fourier transform Raman spectroscopy of carcinogenic polycyclic aromatic hydrocarbons in biological systems: binding to heme proteins. *Journal of Raman Spectroscopy*, 30: 551–555.
78. Farguharson, S., Shende, C., Inscore, F.E., Maksymiuk, P., and Gift, A. (2005) Analysis of 5-fluorouracil in saliva using surface-enhanced Raman spectroscopy. *Journal of Raman Spectroscopy*, 36: 208–212.
79. Li, X., Lin, J., Ding, J., Wang, S., Liu, Q., and Qing, S. (2004) Raman spectroscopy and fluorescence for the detection of liver cancer and abnormal liver tissue, Annual Inter Conf IEEE EMBS, San Francisco, September 1–5.

80. Hanlon, E.B., Manoharan, R., Koo, T.-W., Shafer, K.E., Motz, J.T., Fitzmaurice, M., Kramer, J.R., Itzkan, I., Dasari, R.R., and Feld, M.S. (2000) Prospects for in vivo Raman spectroscopy. *Physics in Medicine and Biology*, 45: 1–59.
81. Shetty, G., Kedall, C., Shepherd, N., Stone, N., and Barr, H. (2006) Raman spectroscopy: evaluation of biochemical changes in carcinogenesis of oesophagus. *British Journal of Cancer*, 94: 1460–1464.
82. Wood, B.R., Quinn, M.A., Burden, F.R., and McNaughton, D. (1996) An investigation into FT-IR spectroscopy as a bio-diagnostic tool for cervical cancer. *Biospectroscopy*, 2: 143–153.
83. Wu, J.-G., Xu, Y.-Z., Sun, C.-W., Soloway, R.D., Xu, D.-F., Wu, Q.-G., Sun, K.-H., Weng, S.-F., and Xu, G.-X. (2001) Distinguishing malignant from normal oral tissues using FTIR fiber-optic techniques. *Biopolymer (Biospectroscopy)*, 62: 185–192.
84. Wong, P.T.T., Papavassiliou, E.D., and Rigas, B. (1991) Phosphodiester stretching bands in the infrared spectra of human tissues and cultured cells. *Applied Spectroscopy*, 45: 1563–1567.
85. Huang, Z., McWilliams, A., Lui, M., McLean, D.I., Lam, S., and Zeng, H. (2003) Near-infrared Raman spectroscopy for optical diagnosis of lung cancer. *International Journal of Cancer*, 107: 1047–1052.
86. Stone, N., Kendall, C., Smith, J., Crow, P., and Barr, H. (2004) Raman spectroscopy for identification of epithelial cancers. *Faraday Discussions*, 126: 141–157.
87. Agarwal, R., Tandon, P., and Gupta, V.D. (2006) Phonon dispersion in poly (dimethylsilane). *Journal of Organometallic Chemistry*, 691: 2902–2908.
88. Laska, J. and Widlarz, J. (2005) Spectroscopic and structural characterization of loe molecular weight fractions of polyaniline. *Polymer*, 46: 1485–1495.
89. Lau, D.P., Huang, Z., Lui, H., Man, C.S., Berean, K., Morrison, M.D., and Zeng, H. (2003) Raman spectroscopy for optical diagnosis in normal and cancerous tissue of the nasopharynx—Preliminary findings. *Lasers in Surgery and Medicine*, 32: 210–214.
90. Frank, C.J., McCreecy, R.L., and Redd, D.C.B. (1995) Raman spectroscopy of normal and diseased human breast tissues. *Analytical Chemistry*, 67: 777–783.
91. Ruiz-Chica, A.J., Medina, M.A., Sanchez-Jimenez, F., and Ramirez, F.J. (2004) Characterization by Raman spectroscopy of conformational changes on guanine-cytosine and adenine-thymine oligonucleotides induced by aminooxy analogues of spermidine. *Journal of Raman Spectroscopy*, 35: 93–100.